Journal of Molecular Structure 1322 (2025) 140466

Contents lists available at ScienceDirect

Journal of Molecular Structure

journal homepage: www.elsevier.com/locate/molstr

Synthesis, characterization, anxiolytic and anticonvulsant activity, DFT, molecular docking, DMPK studies of chalcone derived from maleic anhydride

Francisco N.M. Lucio [a], Akenaton O.C.V. Gomes [d], Paulo N. Bandeira [e], Maria K.A. Ferreira [d], Walber H.F. Ribeiro [e], Ivana C. Romão [d], Caio H.A. Roberto [d], Marcia M. Marinho [e], Alexandre M.R. Teixeira [a,b,c,d], Emmanuel S. Marinho [d], Andreia F.C. de Gomes [f], Jane E.S.A. de Menezes [d], Hélcio S. dos Santos [a,b,d,e,*]

[a] State University of Ceara, Graduate Program in Biotechnology, Fortaleza, CE, Brazil
[b] Department of Biological Chemistry, Regional University of Cariri, Crato, CE, Brazil
[c] State University of Ceará, Campus FAFIDAM, Limoeiro do Norte, CE, Brazil
[d] Science and Technology Center, Graduate Program in Natural Sciences, State University of Ceará, Fortaleza, CE, Brazil
[e] Center for Exact Sciences and Technology - Chemistry Course, Vale do Acaraú University, Sobral, CE, Brazil
[f] Center of Molecular and Environmental Biology, University of Minho, School of Sciences, Department of Biology, Braga, Portugal

ARTICLE INFO

Keywords:
Chalcone
DFT
Anxiolytic
Anticonvulsant
Molecular Docking
Zebrafish
GABAA

ABSTRACT

Anxiety typically doesn't cause convulsions, but intense stress can reduce the threshold for convulsive bouts in predisposed individuals. Chalcones are known to act directly on the central nervous system (CNS) and the presence of electron donor and acceptor groups attached to the aromatic rings in various positions can alter the properties of the molecule. Thus, this work investigated the anxiolytic and anticonvulsant potential of the new chalcone derivative (*E*)-6-(4-((*E*)-3-(3-nitrophenyl)acryloyl)phenyl)-5-oxohex-2-enoic acid (CAMEL). ^{1}H and ^{13}C NMR and ATR-FTIR analyses helped to determine the molecular structure of this chalcone. The energy gap analysis and the higher hardness values than the softness values confirm the stability of CAMEL, with CGDRs indicating that it is more electrophilic in nature. In relation to its potential anxiolytic effect, the tested dose of 40 mg kg^{-1} of the derivative showed behavior like Diazepam, with activity via GABAA. In addition, the derivative also exhibited a possible anticonvulsant effect at the dose of 20 mg kg^{-1}, being like Diazepam, showing involvement in stages 2 and 3 of GABAA receptors in this process. Given the anxiolytic and anticonvulsant activity shown in vivo and *in silico* tests, CAMEL is a promising candidate for the treatment of diseases that affect the CNS.

1. Introduction

Although anxiety is not the direct cause of seizures, it has a significant influence on neural functioning and excitability. In situations of extreme anxiety and stress, the central nervous system (CNS) becomes more susceptible to changes in its electrical activity [1]. This is due to anxiety lowering the threshold required for the manifestation of seizures, especially in predisposed individuals. Furthermore, anxiety is a common comorbidity in patients with epilepsy, with incidence rates reported at around 25 % of cases, where the severity of epileptic seizures is strongly correlated with the presence of anxiety disorders [2]. From this perspective, anxiety is a factor that facilitates the occurrence of seizures in people who are vulnerable. It is therefore important to consider the role of anxiety and stress in the management of patients predisposed to seizures, since reducing these factors can help control seizures and thus provide patients with a better quality of life.

Zebrafish (*Danio rerio*) are used in behavioral neuroscience, including research involving the brain and psychopharmacology. This fish is a suitable model to study the central nervous system because its genotype has 70 % homology with mammalian neurotransmitter receptors. Because of the side effects associated with allopathic drugs, there is a growing interest in the development of alternative therapies to

* Corresponding author at: Center for Exact Sciences and Technology - Chemistry Course, Vale do Acaraú University, Sobral, CE, Brazil.
E-mail address: helcio_santos@uvanet.br (H.S. dos Santos).

https://doi.org/10.1016/j.molstruc.2024.140466
Received 23 May 2024; Received in revised form 16 October 2024; Accepted 19 October 2024
Available online 21 October 2024

treat psychiatric disorders [3]. In view of the considerations, it is important that new strategies, such as the synthesis of new compounds, which can be made available as a viable strategy to deal with various mental disorders, especially anxiety.

Chalcones are open chain flavonoids that are characterized by two aromatic rings joined by a three-carbon α,β-unsaturated carbonyl system. These compounds can be isolated from natural sources due to their widespread distribution in fruits, vegetables, and tea or they can be synthesized by chemical processes [4]. Over the last several years, chalcones have instigated the interest of chemical and pharmacological researchers due to their simple chemical structure and varied biological activities. The chalcone biological activity spectrum includes antinociceptive [5,6], anti-inflammatory [7–9], antitumor [10,11], antibacterial [12], anxiolytic [13], antifungal [14,15], antileishmanial [16], and antioxidant activity [17]. This wide range of activity is mainly due to the numerous substitution possibilities on the chalcone aromatic rings [18].

The nitro group is a versatile and unique functional group in medicinal chemistry. It possesses a strong electron attracting ability that creates localized electron deficient sites within molecules and interacts with biological nucleophiles present in living systems, such as proteins, amino acids, nucleic acids, and enzymes. The interaction can occur by nucleophilic addition and electron transfer involving oxidation and reduction, or also simply by molecular complexation, to induce desired or undesired biological changes [19]. Owing to this, numerous medicinal chemistry campaigns have been initiated to investigate compounds containing nitro groups. As such, drugs containing nitro groups have a long history of use as antineoplastic [20], antibiotic, [21,22] and antiparasitic agents [23,24] as well as tranquilizers, fungicides, insecticides, and herbicides [25].

In this work, the compound (*E*)−6-(4-((E)−3-(3-nitrophenyl) acryloyl)phenyl)−5-oxohex-2-enoic acid ($C_{21}H_{17}NO_6$, hereafter named CAMEL) was synthesized and the molecular structure was characterized by spectroscopy methods, and the Density Functional Theory was used to determine the electronic and reactivity properties. Furthermore, in vivo experiments using the zebrafish (*Danio rerio*) animal model were performed to investigate the anxiolytic and anticonvulsant potential.

2. Material and methods

2.1. General procedures

The chemical reagents were purchased from Sigma-Aldrich. ^{1}H and ^{13}C NMR spectra were obtained using a Bruker Spectrometer, model Avance DPX- 600. The spectra were measured in DMSO solvents, and chemical shifts are reported as δ values in parts per million (ppm. The infrared transmittance spectrum of the chalcone was measured. Attenuated Total Reflectance Fourier Transform Infrared spectroscopy (ATR-FTIR) was performed using a Bruker vacuum infrared spectrometer (FTIR) VERTEX 70 V at room temperature in the range 130 to 4000 cm^{-1}, with a resolution of 2 cm^{-1}.

2.2. Synthesis of the chalcone

The procedure description of the chalcone synthesis is shown in Scheme 1. At ethanol solution of chalcone (*E*)−1-(4-aminophenyl)−3-(3-nitrophenyl)prop-2-en-1-one (1 mmol) was added to a solution of maleic anhydride (1 mmol). The solid that formed was filtered under reduced pressure, washed with cold water solution, and analyzed by TLC.

2.3. Drugs and reagents

The following substances were used: Diazepam (DZP, Neo Química ®) and Dimethylsulfoxide (3 % DMSO; Dynamic®).

2.4. Zebrafish

Zebrafish (*Danio rerio*) (90 to 120 days old; 0.4 ± 0.1 g, 3.5 ± 0.5 cm), wild-caught, of both sexes, were bought from a local store (Fortaleza, CE). The fish were kept in a glass aquarium (30 × 15 × 20 cm) of 10 L ($n = 3$/L), at a temperature of 25 ± 2 °C, under a 24-hour light-dark cycle with chlorinated water solution (ProtecPlus®) and an air pump with submerged filters, at a temperature of 25 °C and pH 7.0, with a 10 to 14-hour circadian cycle (light/dark). The fish were fed Spirulina® food ad libitum 24 h before the experiments. Before administering the medications, the fish were anesthetized in ice-cold water, and after the experiments, they were euthanized by immersion in ice-cold water solution (2 and 4 °C) for 1 min until opercular movements ceased. The work was approved by the Ethics Committee on Animal Use of the State University of Ceará (CEUA-UECE; no. 04,983,945/2021), in accordance with the Ethical Principles of Animal Experimentation.

2.5. General protocol

The Zfa of both sexes were randomly selected in the experiments, anesthetized in cold water solution, and transferred to a damp sponge, treated with 20 μL of the samples (4, 20, and 40 mg kg^{-1}) or Diazepam (4 mg kg^{-1}), or 3 % DMSO (control group - drug diluent) via intraperitoneal (i.p). Then, the animals were individually placed in a glass beaker (250 mL) containing 150 mL of aquarium water solution and kept at rest. For intraperitoneal treatments (i.p.), insulin syringes (0.5 mL; UltraFine® BD) with a 30 G needle were used, and for oral treatments, an automatic monocal micropipette (10 - 100 μL) was used.

2.6. Locomotor activity (Open field test)

The animals were treated with the test samples and subjected to the open field test to assess whether there was a change in motor coordination, either by sedation and/or muscle relaxation. Zebrafish ($n = 6$ / group) were treated, intraperitoneally (i.p.), with 20 μL of sample solutions in doses (4, 20 and 40 mg kg^{-1}) and vehicle (DMSO 3 %) and diazepam (40 mg kg^{-1}). After 30 min of the treatments, the animals were added in Petri dishes containing the same water solution from the aquarium, marked with quadrants, and the locomotor activity was analyzed by counting the number of crossing lines for 5 min [13].

2.7. Toxicity in adult zebrafish (ZFa)

A 96-h acute toxicity assessment was performed using adult zebrafish according to the guidelines of the Organization for Economic Cooperation and Development. Animals ($n = 6$/group) were treated orally (20 μL) with CAMEL (4.0, 20 or 40 mg kg^{-1}) or vehicle (Control; DMSO 3 %). After treatment, the animals were left to rest to analyze mortality rates.

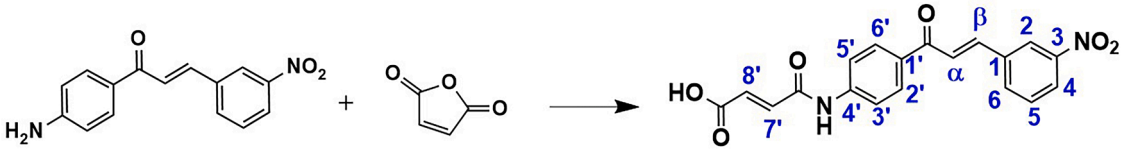

Scheme 1. Synthesis for the chalcone CAMEL.

From 24 h to 96 h, the number of dead fish in each group was recorded, and the lethal dose capable of killing 50 % of the animals (LD50) was determined using the mathematical method trimmed Spearman-Karber with 95 % confidence intervals [26].

2.8. Anxiolytic activity

2.8.1 Light & dark test

The test was carried out in a glass aquarium (30×15×20 cm) with a light and a dark zone, filled with 3 cm of anti-chlorinated and drug-free water solution [15]. The animals (n = 6 / group) were treated intraperitoneally with 20 μL of CAMEL with all those analyzed in the open field test (4.0; 20 or 40.0 mg kg^{-1}), vehicle (DMSO 3 %) and Diazepam (4 mg kg^{-1}). After 30 min, the animals were individually added to the clear area of the aquarium, and the anxiolytic-like effect was quantified as time (s) of stay in the clear area during 5 min of analysis. The lowest active dose was used to assess the mechanism via the GABAergic system [13].

2.8.2 Involvement in the Gabaergic system in anxiolytic activity

The animals (n = 6 / group) received flumazenil intraperitoneally (4 mg kg^{-1}; 20 μL; *i.p.*) and after 15 min were treated with AMOSTRA (20 mg / mL; 20 μL; *i.p.*), Diazepam (40 mg kg^{-1}; 20 μL; *i.p.*), vehicle (3 % DMSO; 20 μL; *i.p.*). After 30 min of the treatments, the animals were submitted to the light & dark test.

2.9. PTZ-induced seizure

Reversal of PTZ-induced seizures has been investigated previously (Siebel et al., 2015). Animals (n = 6/group) were treated with CAMEL (4.0; 20 or 40.0 mg kg^{-1};20 μL; *i.p.*), DZP (4 mg kg^{-1}; 20 μL; *i.p.*), and vehicle (3 % DMSO; 20 μL; *i.p.*). An untreated group (n = 6) was included (naive group). After 30 min, animals were individually exposed to 10 mM PTZ, dissolved in water solution in a 250 mL beaker, and the seizure-like behavior in three stages was evaluated: stage I, drastic increase in swimming activity; stage II, swirl behavior; and stage III, seizures similar to clonus, followed by loss of posture when the animal fell to the side and remained immobile for 1–3 s. At the end of the evaluation of the three stages of the test, animals were euthanized on ice. The mechanism of action was evaluated further [27].

2.9.1. Involvement of the GABAergic system in seizures

The fish (n = 6/group) received flumazenil (4 mg kg^{-1}; 20 μL; *i.p.*). After 15 min, they were treated with CAMEL (40 mg kg^{-1}; 20 μL; *i.p.*) anticonvulsant, DZP (4 mg kg^{-1}; 20 μL; *i.p*), and vehicle (3 % DMSO; 20 μL; *p.o.*). After 30 min of treatment, the animals were individually exposed to PTZ 1(0 mM) and the three stages of seizure were evaluated as described above [13].

2.10. Statistical analysis

The results were expressed as values of the mean ± standard error for each group of 6 animals. After confirming the normal distribution and homogeneity of the data, the differences between the groups were subjected to analysis of variance (one-way ANOVA), followed by the Tukey test. All analyzes were performed using the GraphPad Prism v software. 5.01. The level of statistical significance was set at 5 % ($p < 0.05$)

2.11. Quantum chemical computational calculations

The Density Functional Theory (DFT) method was used for the quantum mechanical calculations. The calculations were performed with the B3LYP [28-36] hybrid functional level of theory and the Pople 6–311++G(d,p) basis set, using Gaussian 09 software [37]. The chalcone CAMEL was optimized in a vacuum and in water solution as a polar implicit solvent, the dielectric constant (ε) of which has a value of 75.56. The solvation study was carried out to investigate the contribution of polar solvent to structural and electronic properties. The solvation model used in the study was the Integral Equation Formalism – Polarizable Continuum Model (IEF-PCM) [38]. A conformational analysis was performed on the optimized structure to obtain the potential energy surface (PES).

The theoretical infrared frequency modes were calculated in a vacuum under conditions of 298.16 K and 1 atm. Additionally, a scaling factor of 0.965 was applied to the calculated vibrational frequencies. The vibrational assignments of the infrared spectrum were based on the Potential Energy Distribution (PED), with only assignments having a PED ≥ 10 being considered. The Gauge-Independent Atomic Orbital (GIAO) approach was used to calculate the isotropic chemical shift of ^{1}H e ^{13}C NMR. The relationship between the experimental and theoretical data was determined by comparing the theoretical shielding constants of hydrogens ($\sigma_{H(calc)}$) and carbons ($\sigma_{C(calc)}$) (calculated for these atoms) with the constants of the same elements in the reference compound tetramethylsilane (TMS), according to the following rule: $\delta_{H(TMS)} - \delta_{H(calc)}$ and $\delta_{C(TMS)} - \delta_{C(calc)}$.

To understand the electronic distribution on the molecule, the Frontier Molecular Orbitals (FMO) were calculated. The chemical behaviour of the chalcone CAMEL can be investigated from the energy values of these orbitals, which in turn were used to calculate the chemical reactivity descriptors: Energy GAP (E_{GAP}, Eq. (1)) [39], Ionization Potential (I, Eq. (2)) [40], Electron Affinity (A, Eq. (3)) [41], Electronegativity (χ, Eq. (4)) [42,43], Global Hardness (η, Eq. (5)), Global Softness (S, Eq. (6)) [44-46], Electrophilicity Index (ω, Eq. (7)) [44] e Nucleophilicity Index (ε, Eq. (8)) [48]. Finally, the molecular electrostatic potential (MEP) was calculated to analysis the charge distribution of the three-dimensional molecular structure.

$$E_{GAP} = E_{LUMO} - E_{HOMO} \tag{1}$$

$$I = -E_{HOMO} \tag{2}$$

$$A = -E_{LUMO} \tag{3}$$

$$\chi = \frac{I + A}{2} \tag{4}$$

$$\eta = \frac{I - A}{2} \tag{5}$$

$$S = 1/\eta \tag{6}$$

$$\omega = \chi^2/2\eta \tag{7}$$

$$\varepsilon = 1/\omega \tag{8}$$

The Condensed Fukui functions were calculated by analyzing Hirshfeld charge population in two situations, one for nucleophilic attack susceptibility (f_A^+, Eq. (9)) and the other for electrophilic attack susceptibility (f_A^-, Eq. (10)). Dual descriptor (Δf, Eq. (11)) was calculated simultaneously with the multiphilic descriptor ($\Delta\omega$, Eq. (12)) to estimate both nucleophilic and electrophilic atomic centers at the same time. If Δf and $\Delta w < 0$, the reactive site has a nucleophilic character. If Δf and $\Delta w > 0$, the reactive site has an electrophilic character. Molecular Electrostatic Potential was calculated and rendered to investigate reactivity sites and how increasing the dielectric constant affects the electronic density distribution in the analyzed structure.

$$f_A^+ = q_N^A - q_{N+1}^A \tag{9}$$

$$f_A^- = q_{N-1}^A - q_N^A \tag{10}$$

$$\Delta f = f^+ - f^- \tag{11}$$

$$\Delta\omega = \omega\Delta f \tag{12}$$

2.12. Docking studies

2.12.1. Docking of the anxiolytic effect on the GABAergic system

To conduct a theoretical evaluation of the anticonvulsant and anxiolytic activities of CAMEL, the methodology described by da Silva et al. (2022) [38] was followed. The protein structures were obtained from the RCSB Protein Data Bank virtual repository (https://www.rcsb.org/) and were subsequently prepared for molecular docking simulations using the AutoDockTools™ version 1.5.6 – MGL Tools© software (https://autodock.scripps.edu/). The structure of carbonic anhydrase II (CAII), identified as 'Coumarins are a novel class of suicide carbonic anhydrase inhibitors,' classified as a lyase in Homo sapiens (with a resolution of 2.0 Å), is deposited on the server under PDB code 3F8E [39]. Meanwhile, the structure of the GABAAR receptor, identified as 'CryoEM structure of human full-length alpha1beta3gamma2 L GABA (A)R in complex with diazepam (Valium), GABA and megabody Mb38′ and classified as a membrane receptor in the organisms Homo sapiens and Escherichia coli (with a resolution of 3.58 Å), is deposited in the database under PDB code 6HUP [40].

In the AutoDockTools™ program, polar hydrogens and Gasteiger charges were added to the protein structures. The grid box was defined to encompass the entire conformational space of the proteins, adjusted to dimensions of 52Åx48Åx61 Å (x,y,z) with coordinates $x = -6.654$, $y = -0.181$, and $z = 16.242$ for the CAII enzyme, and dimensions of 127Åx109Åx126 Å (x,y,z) with coordinates $x = 125.288$, $y = 141.332$, and $z = 135.348$ for the GABAAR receptor. The AutoDockVina™ code was configured to perform a series of 50 independent simulations, each with 30 poses, applying the Lamarckian Genetic Algorithm (LGA) for the CAMEL ligand and the co-crystallized ligands TE1 (CAII inhibitor) and Diazepam (DZP – $GABA_AR$ agonist) [41]. The criterion for selecting the best pose involves the evaluation of statistical and energetic parameters, within ideal limits described in the literature: a Root Mean Square Deviation (RMSD) below 2.0 Å and an affinity energy lower than −6.0 kcal/mol [42].

2.13. In silico DMPK analysis

The quantitative estimation of druglikeness was done by calculating the physicochemical properties of CAMEL on the online server ADMETlab (https://admetmesh.scbdd.com/), which include intrinsic lipophilicity (logP) and at physiological pH (logD at pH 7.4), molecular weight (MW), Topological Polar Surface Area (TPSA), H-bond donor (HBD), and basic pKa. The properties were converted into scoring functions by Pfizer, Inc.'s Central Nervous System Multiparameter Optimization (CNS MPO) algorithm, as shown in Eq. (13), where the desirability score (d) is given by the weighting factor (w) assigned to each physicochemical attribute k, defined by the threshold $T(x)$ formed by the limits: logP ≤ 3, logD ≤ 2, MW ≤ 360 g mol^{-1}, TPSA 40–90 $Å^2$, HBD ≤ 1, and pKa ≤ 8 ($N = 6$). The sum results in a score ranging from 0 to 6 depending on pharmacokinetic viability [42].

$$d = \sum_{i=1}^{N} w_k T_x\left(x_k^0\right) \tag{13}$$

The results were correlated with the predicted descriptors of Parallel Artificial Membrane Permeability Assay (PAMPA) for estimating the Drug Metabolism and Pharmacokinetics (DMPK) profile. The descriptors include apparent permeability (Papp) in colorectal adenocarcinoma 2 (Caco-2) and Madin-Darby Canine Kidney (MDCK) cell lines, passive efflux (Peff), fraction absorbed (%), and volume of distribution (VD), and were predicted using the tools ADMETlab (https://admetmesh.scbdd.com/), PreADMET (https://preadmet.qsarhub.com/), and ADMETboost (https://ai-druglab.smu.edu/admet). The analysis of Human Liver Microsome (HLM) stability was done by predicting the metabolism site on the XenoSite server (https://xenosite.org/), where the 2D probability map was related to the HLM stability descriptors from the ADMETlab (https://admetmesh.scbdd.com/) and ADMETboost (https://ai-druglab.smu.edu/admet) servers, which include substrates of cytochrome P450 (CYP450) isoforms, plasma clearance rate (CLPlasma), hepatic clearance (CLHepa), and Drug-Induced Liver Injury (DILI).

3. Results and discussion

3.1. Geometric optimization and conformational analysis

Chalcones are a subclass of flavonoids characterized structurally by the presence of an α,β-unsaturated carbonyl that separates two aromatic rings, where ring A is directly linked to the carbonyl group and ring B is directly linked to the olefinic β carbon. In this research, the analyzed chalcone derivative (Fig. 1) has a substituent at position 4′ of ring A and 3 of ring B. Ring A is linked to the nitrogen of the carbamoyl group that is part of an unsaturated aliphatic chain (C7′ = C8′) with *E* stereochemistry, containing four carbons and a terminal carboxyl group, and ring B is linked to the NO_2 group. The effect of different environments (vacuum, DMSO, and water solution) was verified on the structural and electronic properties of the chalcone using the DFT method at the B3LYP/6–311++G(d,p) computational level. The structure exhibits low symmetry denoted by the C1 point group, and the presence of the polar nitro and carbonyl groups diametrically opposite to the carbamoyl and carboxylic acid groups numerically decreases the value of the dipole moment (μ) in Debye (D). Solvation environment influences molecular stability, so the calculated dipole moment serves as a parameter for this measure. The higher the dielectric constant, the greater the solvation capacity and separation of partial charges of polar molecules. The increase in the dielectric constant drastically affects the dipole moment of the chalcone ($\mu_{vacuum} = 6.46$ D, $\mu_{DMSO} = 8.35$ D, and $\mu_{water} = 8.38$ D). Thus, the present chalcone has increased structural stability in polar environments, corroborating with literature data [43].

Conformational analysis was carried out on optimized structures using the same computational level, by rotating 20° around the C9' – C1'

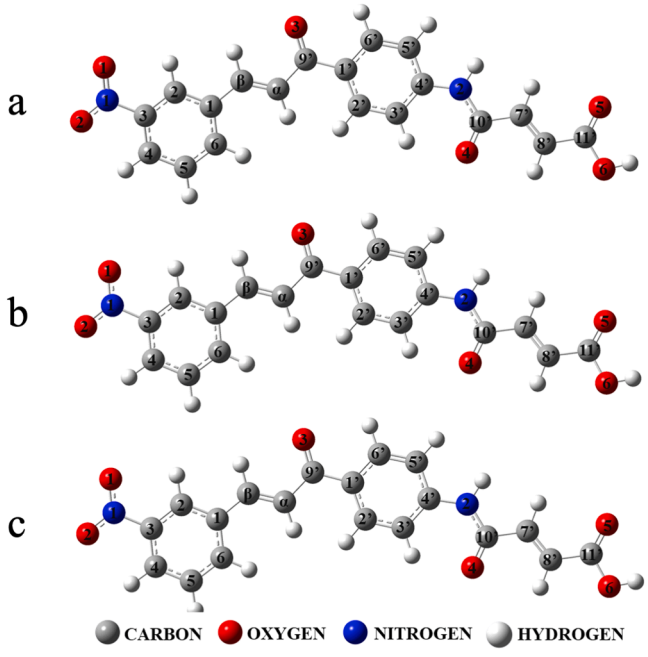

Fig. 1. Optimized three-dimensional structure of the chalcone CAMEL in vacuum (a), DMSO (b) and water solution (c) using the DFT method with the B3LYP/6–311++G(d,p) level of theory.

axis, obtaining the most stable conformer with minima on the Potential Energy Surface (PES). The axis mentioned was chosen to analyze structural stability due to the angle formed by C1' – C9 – Cα (119.0901° in vacuum, 119.0590° in DMSO, and 119.0580° in water solution) being smaller than Cα – Cβ – C1 (123.5452° in vacuum, 123.6159° in DMSO, 123.5144° in water solution), leading to greater steric effects and deviating the structure from planarity. Fig. 2 shows the PES scan, indicating the potential energy minimum via the red dashed line in vacuum (I), DMSO (II), and water solution (III), along with the respective structures of the lowest energy conformers A, B, and C. The global minimum energy conformers show dihedral angles (θ) between the atoms Cα – C9' – C1' – C2' of −8.58° in vacuum, 13.47° in DMSO, and 13.48° in water solution. Also in Fig. 2, the optimized structures of the global minimum conformers in vacuum (I), in DMSO (II) and in water solution (III) are shown, where the red plane contains ring A and the blue plane contains ring B. The global minimum energy conformers in different environments deviate from planarity with the angle γ between rings A and B, corresponding to 11.95° for conformer I, 18.21° for

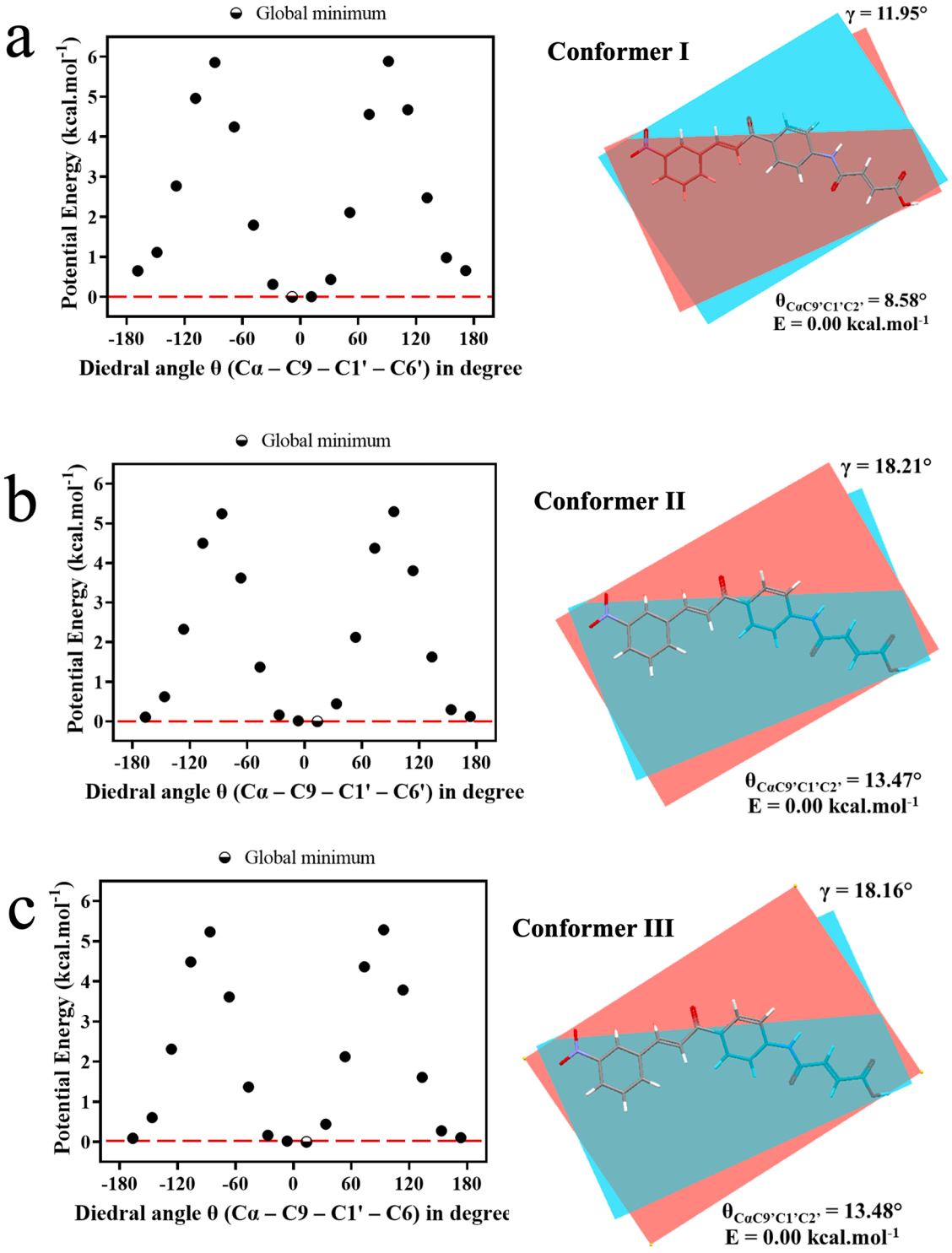

Fig. 2. Potential energy profiles of the chalcone CAMEL calculated in vacuum (a), DMSO (b) and water solution (c) at the B3LYP/6–311++*G*(d,p) level of theory for rotation around Cα-C9-C1'-C6) dihedral angle.

conformer II, and 18.16° for conformer III. In polar environments, there was an increase of 6.26° for conformer II and 6.21° for conformer III in the angle between the rings (γ) compared to conformer I. The analysis of energies in Hartree units indicates that the global minimum conformer obtained in vacuum (E_I = - 1293.5761) is less stable than the global minimum conformers obtained in DMSO (E_{II} = - 1293.6032) and water solution (E_{III} = - 1293.6037).

3.2. Vibrational analysis

Fig. 3a displays the experimental ATR-FT-IR spectra of chalcone. The chalcone CAMEL ($C_{19}H_{14}N_2O_6$) has 41 atoms allowing for 123 degrees of freedom (3N). Therefore, 117 vibrational modes are expected, excluding the three rotational and three translational movements (3N-6). Thus, we highlighted 17 bands in the infrared spectrum, assigned with the help of DFT/B3LYP/6–311++*G*(d,p) calculations and shown in the supplementary material. The linear fit was made using the bands highlighted in Fig. 3a, where it was possible to obtain R^2=0.9929 (Fig. 3b) with the linear equation $y = 0.954x + 100$. These statistical data showed an excellent agreement of the experimental infrared spectrum pools with the bands obtained by theoretical calculations.

In the absorbance ranges between 267 and 967 cm^{-1}, vibrations associated with ring deformations are expected to be observed. The absorbance ranges between 960 and 1671 cm^{-1} mainly comprise stretching modes of CC, CO, CN, and NO as well as deformations of HCC, CCO, and NO atoms. The carbonyl stretching modes (C = O) for chalcones are found in the range of 1594 to 1671 cm^{-1}. In chalcones, it is expected that the carbonyl stretching modes are conjugated with other vibration species, such as the Cα-Cβ stretching mode. OH stretching modes and NO_2 group bending modes appear in the regions between 3700 – 2750 cm^{-1} and 1400 – 700 cm^{-1}, respectively.

3.3. NMR analysis

The ^{13}C NMR (Figure S1) spectra of the chalcone showed a characteristic ketone signal (C = O) conjugated to the *α,β*-unsaturated system with a δ_C value of 191.8 ppm, amide carbonyl at δ_C value of 187.5 ppm and acid carbonyl at δ_C value of 185.9 ppm. Signals were also revealed for C_α with δ_C values of 126.0 and for C_β with δ_C values of 139.0 ppm, which are characteristic of enones. In addition, the C-sp^2 ^1H signals (Figure S2) were observed forming a doublet with coupling values of 7,69 (d, *J* = 16,20 Hz)) for H_α and 8,30 (d, *J* = 15,00 Hz) for H_β, characteristic of *trans* hydrogens. This information justifies the plan for the synthesis of chalcones in the generation of the double bond conjugated to C=O. The ^1H and ^{13}C NMR values are shown in the Table 1 corresponding to the CAMEL. To investigate the theoretical isotropic chemical shifts of ^1H and ^{13}C, tetramethylsilane (TMS) was used as the reference compound. Accordingly, the three-dimensional structure of TMS was optimized using the same level of theory as CAMEL (B3LYP/6–311++*G*(d,p)). The mean value of the isotropic shielding constants calculated for hydrogen and carbon atoms was, respectively: $\sigma_{H(TMS)}$ = 31.9609 ppm and $\sigma_{C(TMS)}$ = 184.6946 ppm. The theoretical chemical shift values showed excellent correlation with the experimental data (Fig. 3c), as demonstrated by the linear fit performed using the calculated isotropic magnetic shifts against the experimental isotropic shifts, with a value of R^2=0.9966, $RMSD_{\delta C}$ =4.97 ppm, $RMSD_{\delta H}$ = 0.73 ppm and linear represented by: $y = 1.017x - 0.8962$.

3.4. Electronic properties

The electronic properties of the molecules of interest can be measured by analyzing the energy and distribution of the FMO to predict the sites most susceptible to electron donation (HOMO) and acceptance (LUMO). Fig. 4 shows the distribution of the HOMO and LUMO orbitals for chalcone. Calculated in vacuum, the HOMO orbital is mainly

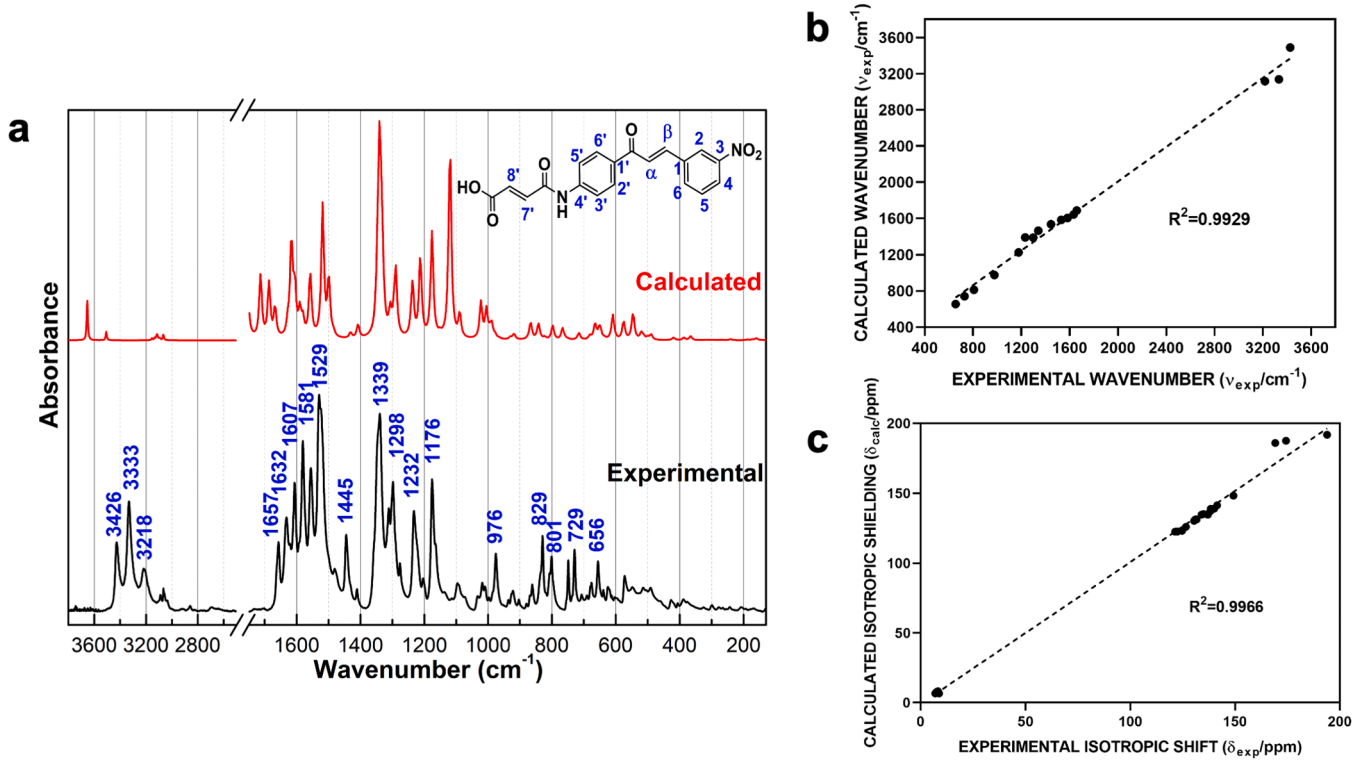

Fig. 3. (a) Experimental ATR-FTIR and theoretical Infrared spectrum obtained at B3LYP/6–311++*G*(d,p) level of theory. (b) the linear correlation of the experimental wavenumbers and theoretical wavenumbers for the fundamental vibrational modes. (c) linear correlation with the experimental ^1H and ^{13}C isotropic shielding and the calculated isotropic magnetic shielding.

Table 1
^{1}H (500 MHz) and ^{13}C (125 MHz) NMR data on (DMSO), δ ppm, J/Hz.

			HSQC		HMBC	
C	$\delta_{C(exp)}$	$\delta_{C(calc)}$	$\delta_{H(exp)}$	$\delta_{H(calc)}$	$^{2}J_{CH}$	$^{3}J_{CH}$
1	134.7	134.9			H-2/H_{β}	H-6
3	148.2	149.2			H-2	
1′	135.1	136.9			H-2′/H-6′	
4′	141.3	141.4				
[a]C=O	191.8	193.9			Hα	H_{β}
[b]C=O	187.5	174.3				
[c]C=O	185.9	169.3				
CH	$\delta_{C(exp)}$	$\delta_{C(calc)}$	$\delta_{H(exp)}$	$\delta_{H(calc)}$	$^{2}J_{CH}$	$^{3}J_{CH}$
2	122.6	122.5	8.69 (s)	8.29		
4	123.1	124.7				
5	130.3	130.4	7.73 (m)	7.54		
6	134.7	133.9	8.20 (d, *J* = 7.8 Hz)	8.20		H-2
2′/6′	131.3	131.3	7.95 (d, *J* = 9.0 Hz)	8.12		
3′/5′	122.5	121.5	6.60 (d, *J* = 8.4 Hz)	6.97		
7′	138.8	138.4				
8′	137.1	138.1				
C_{α}	126.0	126.5	7.69 (d, *J* = 16.20 Hz)	7.95		
C_{β}	139.0	140.1	8.30 (d, *J* = 15.00 Hz)	8.31		H-2

distributed in the binding positions of ring A, carbonyl oxygen, *α,β*-unsaturated portion, and carbamoyl group. The presence of the nitro group does not contribute to the formation of the HOMO isosurface in ring B. The LUMO orbital is distributed throughout the molecule in the anti-binding positions of the π bonds. Thus, we can conclude that the HOMO-LUMO transition occurs between π-π* orbitals. In the calculated polar environments, the formation of the HOMO isosurface occurs in ring B, while the LUMO isosurface is distributed only in ring B and the α,β-unsaturated portion. Therefore, the region with the largest HOMO isosurface can be characterized as the site with the highest electron-donating character (ring A in the calculated environments), and the region with the largest LUMO isosurface can be characterized as the site with the highest electron-accepting character (ring B in the calculated environments). In addition, the analysis of the FMO energy (E_{HOMO} and E_{LUMO}) provides a quantitative parameter for discriminating the electron density donation and acceptance capacity, where the higher the E_{HOMO} value, the higher the donating character, and the lower the E_{LUMO} value, the higher the electron-accepting character. The numerical values of E_{HOMO} (−6.959 eV in vacuum; −6.793 eV in DMSO; −6.791 eV in water solution) increase in polar environments, indicating that in DMSO and water solution, chalcone has a higher electron density donating character. Conversely, in polar environments, there is a slight decrease in the E_{LUMO} values (−3.212 eV in vacuum; −3.217 eV in DMSO; −3.219 eV in water solution), indicating that in DMSO and water solution, chalcone has a higher electron-accepting character. Chemical reactivity analysis can be performed based on the energy gap (ΔE) that measures chemical stability and ease of electronic transitions, where lower ΔE values indicate greater ease for the HOMO-LUMO transition and lower chemical stability, and higher ΔE values indicate less ease for electronic transitions and higher chemical stability. For chalcone, the energy gap values follow the order: vacuum = 3.747 eV > DMSO = 3.576 eV > water solution = 3.572 eV, suggesting that chemical reactivity is higher and electronic transition is facilitated in the calculated polar environments.

Global Chemical Reactivity Descriptors (GCRDs), Table 2, can be calculated through EHOMO and ELUMO and are characterized as an extension of FMO. The analysis of GCRDs provides an excellent indication for proposals of protein-ligand interaction mechanisms. The HOMO orbital is related to the parameters I and ε, which indicate the capacity for electron density donation, while the LUMO orbital is related to the parameters EA, χ, and ω, which indicate the capacity for electron density acceptance. Thus, the results show that an increase in the dielectric constant leads to a decrease in the values of the descriptors: I (vacuum = 6.959 eV > DMSO = 6.793 eV > water solution = 6.791 eV), EA (vacuum = 6.959 eV > DMSO = 6.793 eV > water solution = 6.791 eV), and χ (vacuum = 5.08 eV > DMSO = 5.05 eV > water solution = 5.05 eV), suggesting that the higher the polarity of the medium, the greater the electron donor character and the lower the electron acceptor character of the chalcone. The analysis of the descriptors ω and ε shows a

Table 2
Global Chemical Reactivity Descriptors (GCRDs) for chalcone in the vacuum, DMSO and water solution computed by DFT method using B3LYP/6–311++*G*(d, p) basis set.

Descriptors	Vacuum	DMSO	Water solution
***I* (eV)**	6.959	6.793	6.791
***EA* (eV)**	3.212	3.217	3.219
***χ* (eV)**	5.085	5.005	5.005
***η* (eV)**	1.873	1.788	1.786
***S* (eV^{-1})**	0.534	0.559	0.560
***ω* (eV)**	6.902	7.000	7.013
***ε* (eV^{-1})**	0.145	0.143	0.142

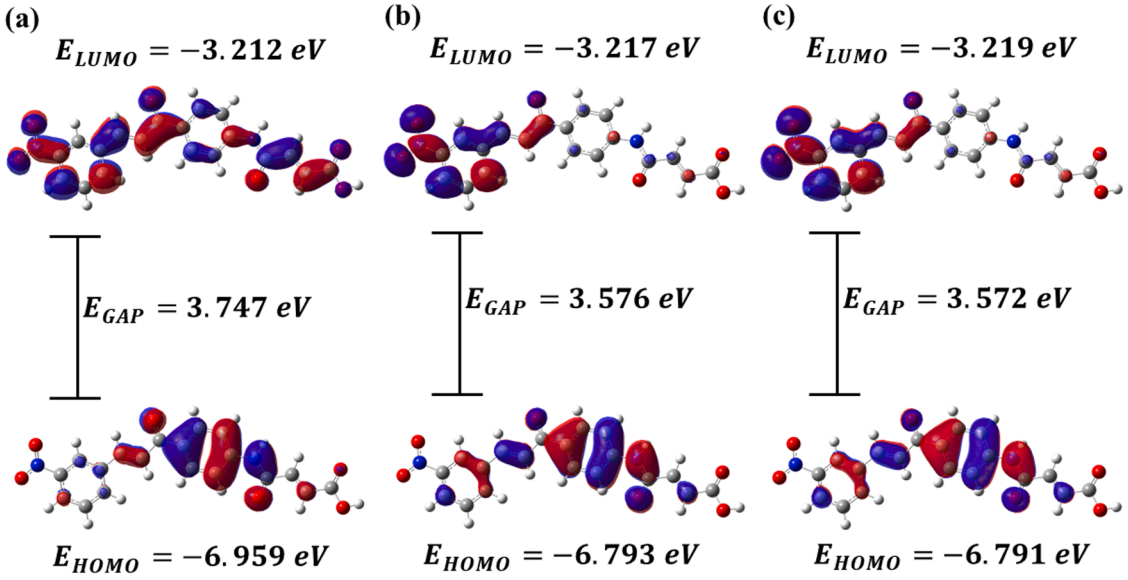

Fig. 4. Distribution of HOMO and LUMO orbitals of the chalcone CAMEL in vacuum (a), DMSO (b) and (c) water solution.

preference in the chemical behavior of the analyzed molecular species; higher ω values and lower ε values indicate that the molecule acts better as an electrophile, conversely, higher ε values and lower ω values indicate better nucleophilic behavior. The results show that in the environments analyzed, the chalcone behaves better as an electrophile (ω = 6.90 eV and ε = 0.145 eV-1 in vacuum; ω = 7.00 eV and ε = 0.143 eV^{-1} in DMSO; ω = 7.00 eV and ε = 0.143 eV^{-1} in water solution). As an extension to the study of chemical reactivity, the descriptors η and S are used to predict the hard or soft character, respectively, of the analyzed chemical species. These parameters follow the principle of maximum hardness (MHP): structures tend to arrange towards higher hardness values. Therefore, the chalcone behaves as a hard chemical species, and an increase in the dielectric constant decreases hardness (η = 1.873 eV in vacuum, η = 1.788 eV in DMSO, and η = 1.786 eV in water solution) and increases softness (S = 0.533 eV^{-1} in vacuum, S = 0.559 eV^{-1} in DMSO, and S = 0.560 eV^{-1} in water solution).

In addition to analyzing the global electronic properties, the condensed Fukui functions (f_A^+ and f_A^-) were calculated using the DFT method at the same theory level, using the Hirshfeld atomic charge population analysis, to understand the chemical behavior of each atom. The positive Fukui function (f_A^+) is related to an atom's susceptibility to undergo a nucleophilic attack (acting as an electrophile), and the negative Fukui function (f_A^-) is related to an atom's susceptibility to undergo an electrophilic attack (acting as a nucleophile). Therefore, the more positive the values of f_A^+ for a given atom, the more electrophilic the behavior, and the more positive the values of f_A^- for a given atom, the more nucleophilic the behavior. Table S1 shows positive values for the functions f_A^+ and f_A^- in different environments, indicating that these atoms exhibit both nucleophilic and electrophilic character, except for atom C7′ (f_A^- = −0.00394) in a vacuum. Although providing important information about the chemical character of each atom, the f_A^+ and f_A^- functions cannot estimate the preference in behavior when atoms have positive values for both functions, requiring further study through the analysis of the dual descriptor (Δf) and multiphilic descriptor ($\Delta\omega$) that estimate the chemical behavior together. The graph in Fig. 5a was plotted based on the $\Delta\omega$ values for each atom obtained from Table S2. According to the results in a vacuum, the atoms with higher nucleophilic character are C1, C2, C3, C4, C5, Cα, Cβ, C1′, C2′, C3′, C4′, C5′, C6′, O4, and N2, while the atoms with higher electrophilic character are C6, C7′, C8′, C9′, C10′, C11′, O1, O2, O3, O5, O6, N1. The carbon atoms in ring A show more negative $\Delta\omega$ values compared to the carbon atoms in ring A, indicating a region with higher nucleophilic character, which can be explained by the presence of the NO_2 group in ring B acting as an electron-withdrawing substituent. The increase in the dielectric constant causes changes in the chemical behavior of each atom; however, when comparing the DMSO and water solution environments, the behavior is similar. In the analyzed polar environments, the carbon atoms in ring B (C1, C2, C3, C4, C5, and C6), the α,β-unsaturated olefinic portion, C7′, C9′, O3, and the nitro group (N1, O1, and O2) show higher electrophilic character, while the carbon atoms in ring A (C1′, C2′, C3′, C4′, C5′, and C6′), C10′, C11′, O3, O4, O5, and N2 show higher nucleophilic character.

3.5. Molecular electrostatic potential

The Molecular Electrostatic Potential (MEP) is a useful tool in understanding protein-ligand interaction sites in biological studies. MEP analysis shows the distribution of electron density for the chalcone through colored surfaces from blue to red, where the electron density increases in the order: blue < green < yellow < orange < red. Blue regions are electron-deficient and interact with nucleophilic species, while red regions are electron-rich and interact with electrophilic species. The MEP for the chalcone in vacuum (I), DMSO (II), and water solution (III) environments is shown in Fig. 5b. In vacuum, oxygen atoms have high electron density due to the high electronegativity, while hydrogen atoms, especially carboxylic hydrogens and the carbamoyl group, have

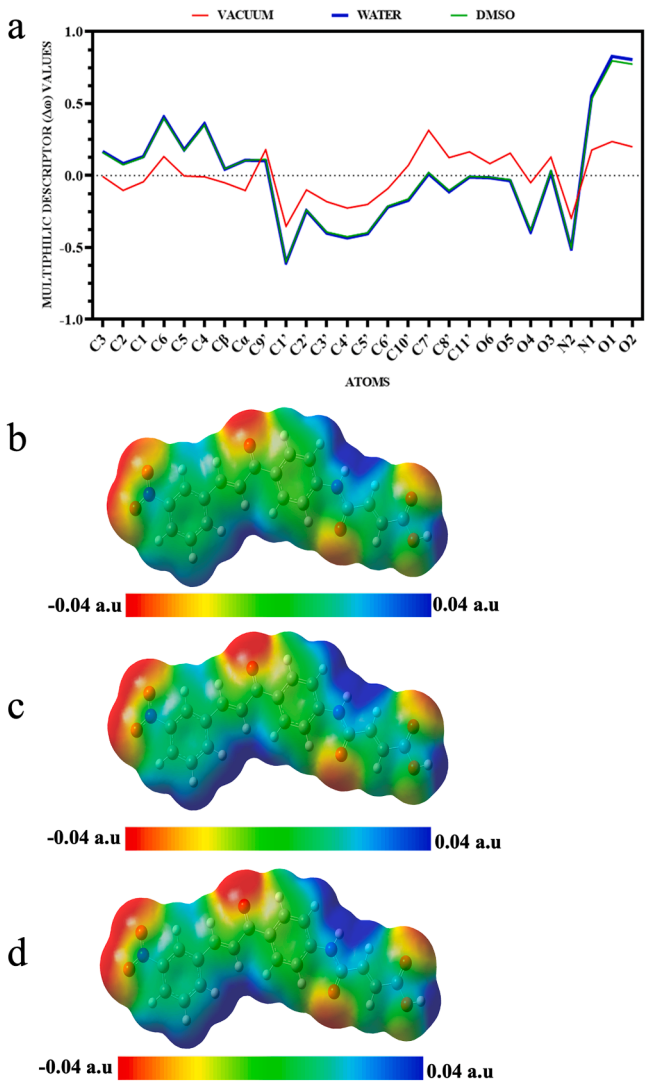

Fig. 5. (a) Multiphilic descriptor ($\Delta\omega$) values for the chalcone CAMEL in the environments: vacuum (red), DMSO (green) and water solution (blue). MEP surfaces plotted in vacuum (b), DMSO (c) and water solution (d), onto the 0.001a.u. isosurface. The MEP values at selected points of the surface are given in a.u.

low electron density. A slightly yellow region appears on the π bonds of ring A. Green regions appear on the π bonds of ring B, α,β-unsaturated olefinic portions, and C7'–C8'. The increase in the dielectric constant of the medium affects the electron density distribution of the chalcone, making regions with high electron density more negative and regions with low electron density more positive. Through the analysis of Δw, we observe that: the N2 atom, despite not showing a negative contour surface, has a high nucleophilic character; the O1 and O2 atoms, with high electron density, behave preferentially as electrophilic centers; and the O4 and O5 atoms, with lower electron density than O1 and O2, behave preferentially as nucleophilic centers. The nucleophilic/electrophilic character generally associated with electron density cannot always be used interchangeably; thus, good nucleophiles will not always have high electron density, and good electrophiles will not always have low electron density.

3.6. Anxiolytic and anticonvulsant

3.6.1. Acute toxicity 96 h

The zebrafish, an animal model gaining more and more space in the

academic world, proposed to be used as the first contact of a substance with an organism, is present in various studies including experiments on toxicities that can be carried out in embryonic, larval, and adult stages. The advantages that make the zebrafish so popular lie in its development, reproduction, handling, cost-effectiveness, and notably, besides its genome similarity to humans, it's almost immediate response to external and internal stimuli, yielding concise and rapid results [44]. Adult zebrafish are used to perform acute toxicity tests on substances under study. The chalcone CAMEL was not toxic to adult zebrafish within a period of up to 96 h of analysis, showing some mortality but not exceeding 50 % of the animals used (LC50 $>$ 1.0 mg/mL), and no anatomical alterations were observed.

3.6.2. *Locomotor activity (Open field test)*

The zebrafish is evaluated based on its behavior, swimming speed, and movement quantification. Therefore, locomotor activity is crucial to analyze and measure the intensity of the substance's effect on the central nervous system of adult zebrafish, causing the necessary stimulus to alter the animal's naturally anxious behavior, with expected attitudes consistent with the desired outcomes [44]. The open field test is appropriate as it defines certain parameters considering the swimming activity of the animal and its movement to determine if there was any restriction in locomotion, resulting in a more static animal or if its swimming pattern remains regular [45]. Recently, we adapted the open field test using Petri dishes to evaluate the locomotor activity of adult zebrafish under the influence of analgesic drugs [46]. The results showed that at the tested doses of 20 and 40 mg kg^{-1} of CAMEL, the behavior differed from DZP ($^{\#}\,^{\#}p < 0.01$, $^{\#}\,^{\#}\,^{\#}p < 0.001$ vs DZP), indicating no alteration in the animal's locomotion (Fig. 6a). All doses showed different behavior compared to the negative control DMSO 3 %

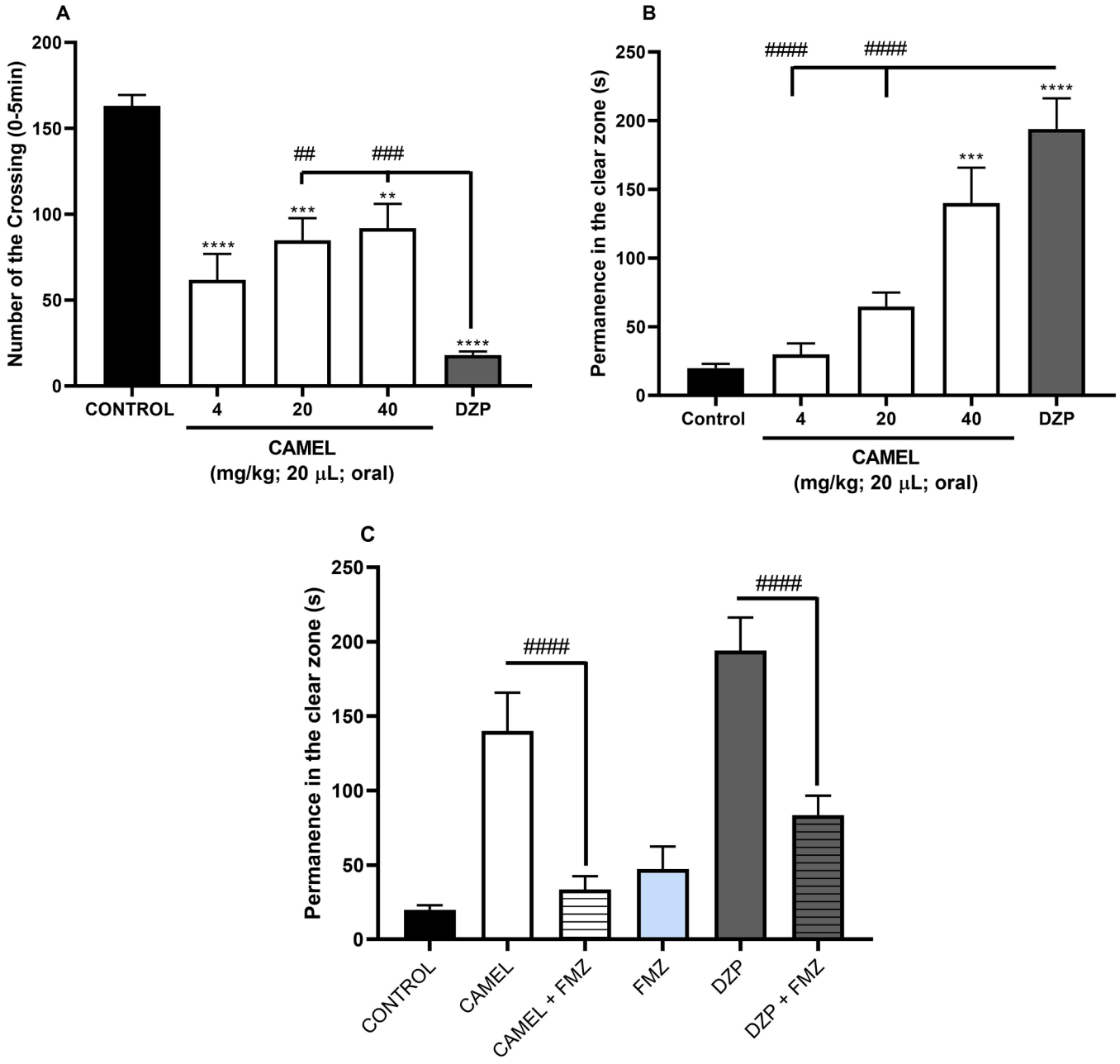

Fig. 6. (a) Effect of the chalcone CAMEL on the locomotor behavior of adult zebrafish in the Open Field Test (0–5 min). (b) Anxiolytic effect of CAMEL on adult zebrafish (*Danio rerio*). (c) Mechanism of anxiolytic action via GABA of the sample CAMEL (40mg kg^{-1}). Values represent the mean ± standard error of the mean for 6 animals/group; ANOVA followed by Tukey's test.

(**$p < 0.01$, ***$p < 0.001$, ****$p < 0.0001$ vs Control), but the 4 mg kg^{-1} (****$p < 0.0001$ vs DZP) dose behaved similarly to DZP, with fish exhibiting a more lethargic behavior.

3.6.3. Anxiolytic activity

Zebrafish, similar to humans and many other species, naturally exhibit anxious behavior, leading them to prefer locations with reduced lighting. This preference is the key parameter driving the Light-Dark test. Based on this behavioral pattern, the level of relaxation or tranquility induced by the substance under analysis is evaluated by observing how long the animal stays in the brightest area of the aquarium. Other factors such as the time taken to move to the dark side of the tank and the number of switches between the light and dark sides of the aquarium are also taken into account. Being responsive to environmental and organismic stimuli, the Light-Dark test, along with toxicity assessment, complement each other in determining whether the substance can cause any immediate anomalies or anatomical alterations in the fish. The results (Fig. 6b) show that only the 40mg kg^{-1} dose of CAMEL exhibited a significant difference from the negative control (DMSO 3 %), indicating a potential reversal of the animal's natural anxious behavior. Furthermore, the 40mg kg^{-1} dose showed similar (***$p < 0.001$ vs DZP) results to the behavior displayed by the positive control Diazepam, suggesting a potential anxiolytic effect with animals spending more time in the bright zone of the aquarium.

3.6.4. GABAergic neuromodulation

Gamma-aminobutyric acid (GABA) is a chemical messenger that transmits information from one neuron to another, regulating the nervous system. It is considered the main inhibitory neurotransmitter in the central nervous system, released by neurons called GABAergic neurons and connecting to specific receptors on other neurons. Among its receptors, the gamma-aminobutyric acid type A (GABAA) receptor is the most widely distributed fast-acting receptor in the central nervous system (CNS) of mammals. GABAA receptors are pentameric transmembrane ion channels and exhibit high heterogeneity among their subunits. When these receptors are activated by the neurotransmitter GABA, they allow chloride ions to pass into neurons, resulting in hyperpolarization of these cells, making them less responsive to excitatory neurotransmitters, meaning that these receptor neurons then undergo a decrease in neuronal conduction, causing inhibition of the nervous system. GABAA receptors are targets of various pharmacological groups with anesthetic and sedative properties (Smith, 2005). Thus, to investigate the mechanism of action of Maleic anhydride derivative (40 mg kg^{-1}) that showed anxiolytic effect (best effective dose in the light/dark test), we analyzed the anxiety neuromodulation mechanism via GABAA. In general, it is expected that during the neuromodulation test, the antagonist flumazenil will block GABAergic receptors, preventing the sample from acting on them. Thus, animals that naturally exhibit anxious behavior continue to display such conduct. In this perspective, the CAMEL (40 mg kg^{-1}, Fig. 6c) had its anxiolytic effect neuromodulated by the GABAA receptor by showing a statistically significant difference between the sample and the sample plus the flumazenil antagonist (CAMEL $^{\#\#\#\#}p < 0.0001$ vs CAMEL + Fmz; Fig 6c), meaning that the anxiolytic effect was blocked by flumazenil.

3.6.5. Pentilenotetrazol-induced convulsion (PTZ)

PTZ acts on the GABAA receptor, blocking the Cl channel, and is commonly used to induce the progressive development of seizures in animal models [47]. Repeated treatment with PTZ is associated with biochemical and histological changes - similar to those observed in epileptic individuals - which are the main contributors to the cognitive and emotional behavioral impairments demonstrated in animal models [47]. The anticonvulsant effect of CAMEL and Diazepam on PTZ-induced seizures in adult zebrafish was investigated. The results show (Fig. 7A-C) that all doses (4, 20, and 40 mg kg^{-1}) of the CAMEL in stage 1 showed similar results to the behavior exhibited by the positive control Diazepam, indicating a potential anticonvulsant effect. In stages 2 and 3, only the dose of 20mg kg^{-1} showed a result similar to DZP, demonstrating a potential anticonvulsant effect, with animals showing a high latency time for the onset of seizures at this stage.

3.6.6. Evaluation of GABAergic neuromodulation

To investigate the mechanism of action of CAMEL (20 mg kg^{-1}) that showed anticonvulsant effect (Best effective dose in the PTZ-induced seizure induction test), we analyzed the seizure neuromodulation mechanism via GABAA. In general, it is expected that during the neuromodulation test, the flumazenil antagonist will block the GABA receptors, preventing the sample from acting on them. Thus, the sample that showed anticonvulsant effect will reveal the opposite result, with fish remaining in less latency time for the onset of seizures in stages representing a convulsive crisis, suggesting a different effect from Diazepam, the positive control. From this perspective, the CAMEL sample (20 mg kg^{-1}, Fig. 8) in all evaluated stages (Stage I (A), Stage II (B), and Stage III (C)) showed shorter latency time to reach the characteristic stages of convulsive crises, occurring due to interference of the $GABA_A$ channel blocker (Flumazenil), indicating that the sample had its anticonvulsant effect neuromodulated by this receptor. In agreement, the sample showed a significant statistical difference between the sample and the sample plus the flumazenil antagonist only in stages 2 and 3 (CAMEL vs. CAMEL + Fmz; ($^{\#}p < 0.05$; $^{\#\#\#\#}p < 0.0001$, Fig. 8), meaning that the convulsive effect caused by PTZ and previously reversed by the sample was blocked by flumazenil.

3.7. Molecular docking

3.7.1. Docking of the anxiolytic effect on the GABAergic system

With the aim of estimating the theoretical anxiety mechanism of the CAMEL ligand, the ligand's modulation potential on the $GABA_AR$ receptor was analyzed (Fig. 9). After the calculations, an RMSD of about 1.747 Å for CAMEL was verified, showing a low root mean square deviation of fitting at the binding site facing the receptor (Table 3). Regarding the location region of CAMEL, it was observed that it complexed with the receptor at the same agonist binding site as DZP, located between chains C and D in the extracellular domain (Fig. 9a) where its affinity energy was measured at around −8.9 kcal/mol (Table 3), while DZP had an affinity energy value of −7.16 kcal/mol (Table 3). This indicates that CAMEL has good specificity for $GABA_AR$. Thus, this analysis suggests that CAMEL energetically complexed more favorably than DZP, indicating that the ligand is a good candidate to act as an agonist for $GABA_AR$ receptors. Regarding the interactions that the ligand formed with the binding site residues, it was possible to observe that CAMEL formed six hydrophobic interactions with the residues Tyr-58C, Phe-77C, Asn-103D, and Thr-142C, two of which were common with DZP in relation to the aromatic side chain of Tyr-58C and Phe-77C [27] (Fig. 9e). Both through their aromatic structures (Fig. 9b-c), four hydrogen bonds were observed between CAMEL and polar side chain residues Asn-60C and Ser-195C, and we can also highlight two interactions: a parallel π-Stacking interaction at a distance of 4.49 Å with the aromatic side chain residue Phe-77C, and a salt bridge interaction (5.48 Å) with the positively charged side chain residue Lys-156D (Table 3). These analyses suggest that CAMEL can act on GABAAR receptors similarly to DZP.

3.7.2. Docking of the anticonvulsant effect

With the aim of estimating the theoretical mechanism of action of CAMEL anticonvulsant effect, the binding potential against the CAII enzyme was analyzed (Fig. 9). After the molecular docking calculations were completed, it was observed that the ligand bound to the enzyme at the same binding site as the TE1 inhibitor (Fig. 9f), showing an RMSD deviation of around 1.858 Å (Table 3), indicating that the simulations performed within an ideal statistical threshold allowing for reproducibility of the simulation model. With the formation of the CAMEL-CAII

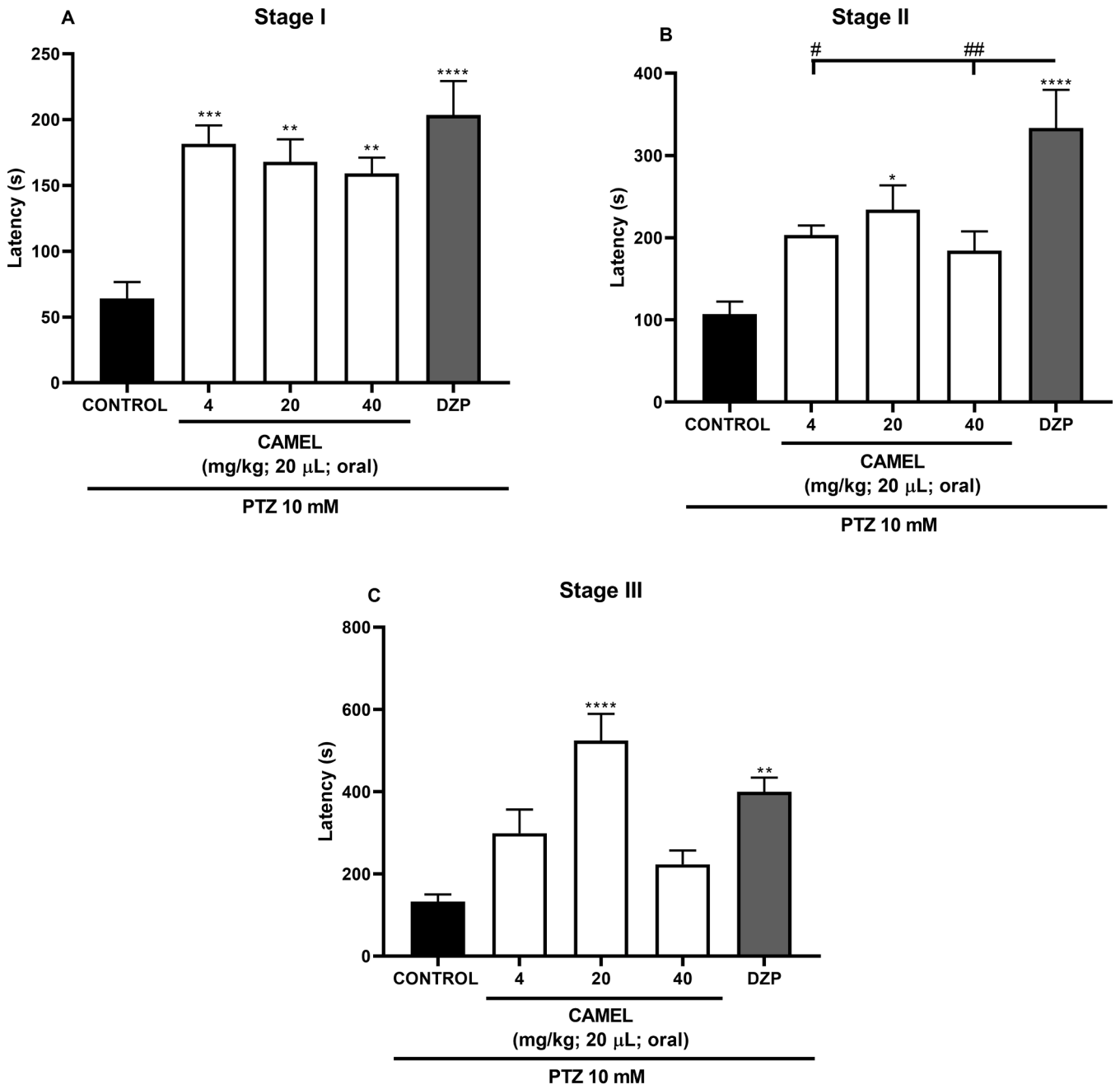

Fig. 7. Anticonvulsant test for chalcone CAMEL (A) Stage I. (B) Stage II (C) Stage III. Anticonvulsant effect of the sample in adult zebrafish (*Danio rerio*) from seizure induction by PTZ. Values represent the mean ± standard error of the mean (E.P.M.) for 6 animals/group; ANOVA followed by Tukey.

complex, the affinity energy was measured at around −7.1 kcal/mol (Table 3), compared to the affinity energy measured for the inhibitor after redocking calculations, which was around −5.4 kcal/mol (Table 3), showing better specificity. Regarding the ligand-protein interactions, it was noted that CAMEL formed six hydrophobic interactions with the residues Ile-91, Gln-92, Asp-130, Phe-131, Leu-198, Thr-199, Thr-200, His-94, and His-96 (Table 3), with two in common with the co-crystallized inhibitor TE1 in relation to the aliphatic and polar side chain residues Ile-91 and Gln-92 respectively (Fig. 9.g-h). Four hydrogen bonds were observed with the polar side chain residues Gln-92, Thr-199, and Thr-200, with the hydrogen bond with the residue Gln-92 being common with TE1 (Fig. 9. g-h). A π-Stacking interaction was noted in common with TE1 between the aromatic side chain residue Phe-131, where for CAMEL this interaction was parallel and for TE1 it was transversal, highlighting three salt bridge interactions with the positively charged side chain residues His-94, His-96, and His-119 (Table 3). These analyses suggest that CAMEL may act similarly to TE1, as it showed interactions with key residues of the active site (Table 4).

3.8. MPO-based Admet analysis

3.8.1. CNS MPO desirability

For Wager et al. [48], compounds that are not very fat-soluble (logP < 3) and are more polar than active compounds in the CNS (TPSA > 75 $Å^2$), as long as they fall within a range of MW that allows for good metabolic stability (MW 200–500 g mol^{-1}), show a correlation between apparent permeability (Papp in 10^{-5} cm/s) and hepatic clearance (CLHepa < 100 mL/min/kg), ensuring a DMPK viability. An analysis of molecular lipophilicity potential (MLP) can provide information on the

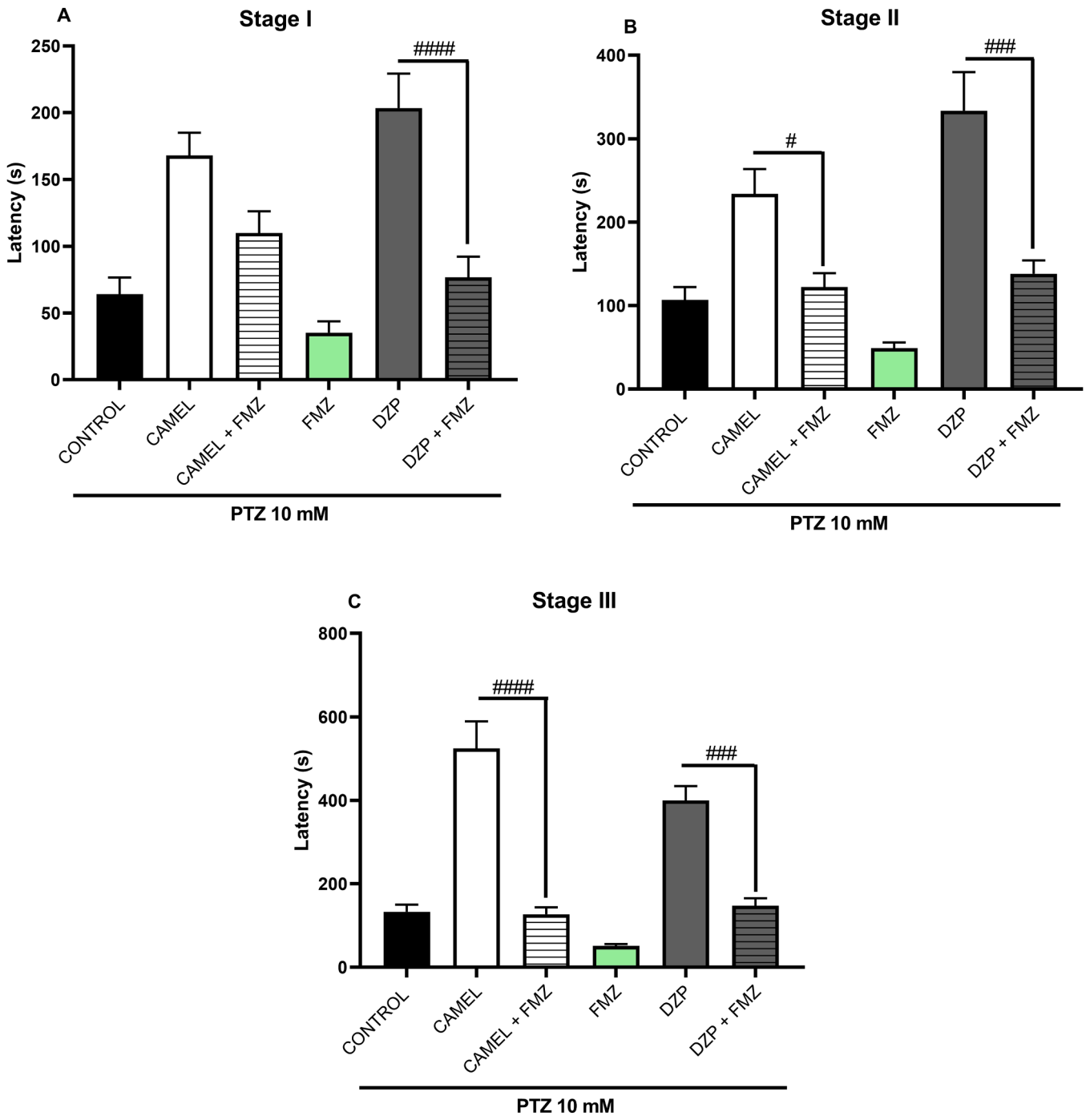

Fig. 8. Mechanism of anticonvulsant action via GABA of the chalcone CAMEL for sample (20mg kg^{-1}) (A) Stage I. (B) Stage II (C) Stage III. (*Danio rerio*) adult in the PTZ seizure induction test. Values represent the mean ± standard error of the mean (S.E.M.) for 6 animals/group. ANOVA followed by Tukey ($^{###}p < 0.001$, $^{####}p < 0.0001$ DZP vs. Fmz + DZP, $^{\#}p < 0.05$, $^{####}p < 0.0001$ CAMEL. vs. Fmz + CAMEL).

lipophilicity and polarity of molecular fragments that either enhance or reduce permeability in the lipid bilayer of small molecules. In a topological analysis of MLP (Fig. 10a), it was observed that the aromatic center formed by aromatic systems (rings A and B), connected by the α,β-unsaturated system, contributes to a molecular surface that is essentially hydrophobic (blue color spectra), while the aliphatic substructure of amide (NHCO) linked to the carboxyl group (COOH) make up the polar surface of CAMEL (69.23 $Å^2$) and thus present a molecular surface that is essentially hydrophilic (red color spectra), resulting in a logP value around 2.60 that expresses the balance between lipophilicity and solubility. In the DMPK viability radar (Fig. 10b), it can be observed that the descriptors of lipophilicity (logP) and polarity (TPSA), when aligned with the calculated MW of 366.33 g mol^{-1}, fall within an ideal spectrum predicted by the CNS MPO algorithm, where a score of 4.3 (on a scale of 0 to 6) indicates that the alignment between the physicochemical attributes of CAMEL basically meets the criteria of Pfizer, Inc.'s biopharmaceutical classification system.

3.8.2. Parallel artificial membrane permeability assay (PAMPA) descriptors

For estimating the cell permeability profile in the intestinal and brain environments, the descriptors of the Parallel Artificial Membrane

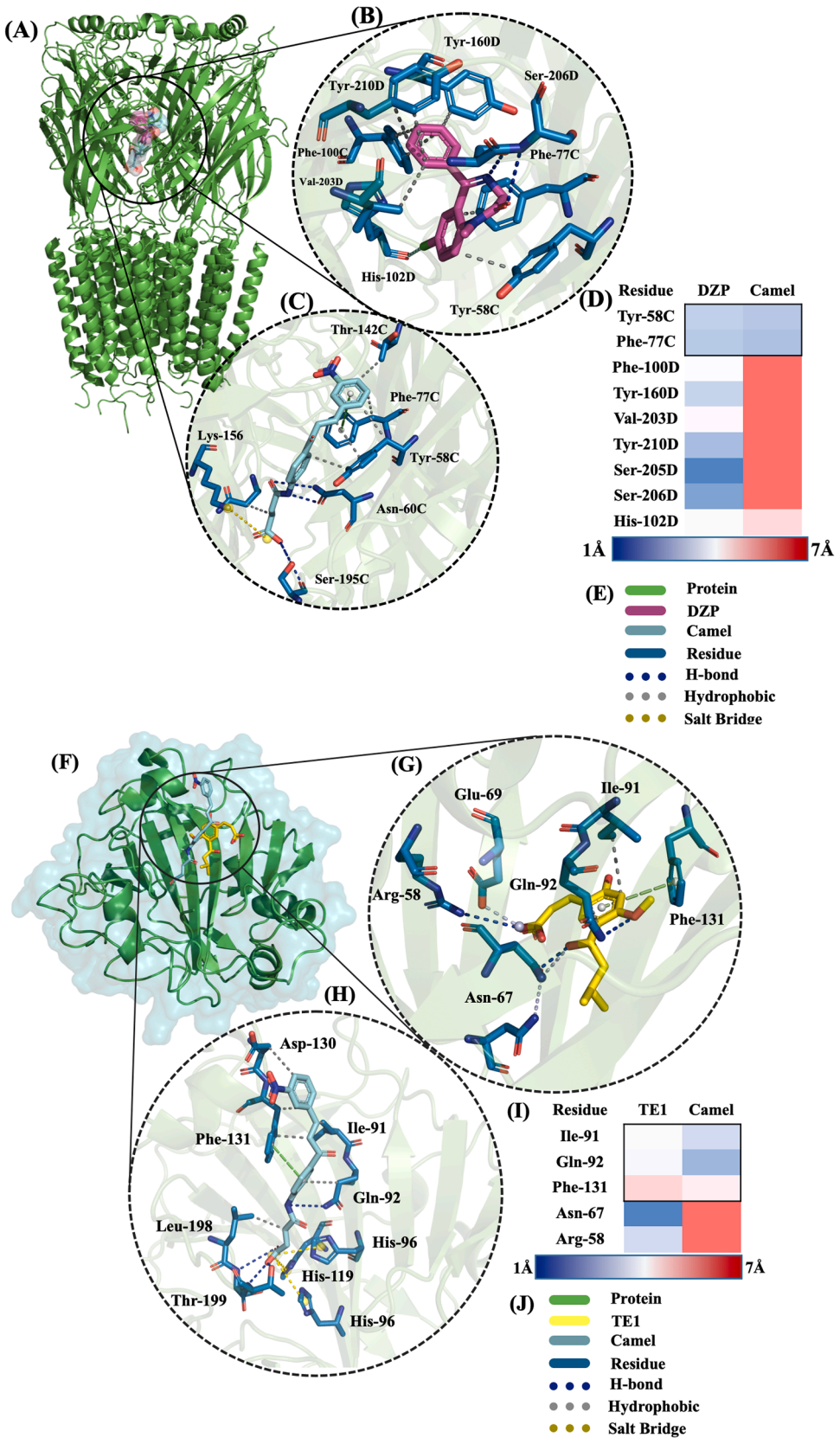

Fig. 9. Complex of the $GABA_AR$ receptor with ligands DZP (purple) and CAMEL (cyan), and the CAII receptor with ligands TE1 (yellow) and CAMEL (cyan).

Table 3
Data from molecular docking calculations between the CAMEL ligand and $GABA_AR$ and CAII targets expressed in RMSD and affinity energy, and details of ligand-protein interactions expressed in interaction type, amino acid residue, and distance from interactions.

Ligand	Target	Affinity energy (kcal/mol)	RMSD (Å)	Residue	Interactions Type	Distance (Å)
CAMEL	$GABA_AR$	−8.9	1.747	Tyr-58C	Hydrophobic	3.46
				Tyr-58C	Hydrophobic	3.68
				Tyr-58C	Hydrophobic	3.51
				Phe-77C	Hydrophobic	3.42
				Asn-103D	Hydrophobic	3.77
				Thr-142C	Hydrophobic	3.57
				Asn-60C	H-bond	3.08
				Asn-60C	H-bond	2.56
				Ser-195C	H-bond	3.23
				Ser-195C	H-bond	3.33
				Phe-77C	π-Stacking-P	4.49
				Lys-156D	Salt Bridge	5.48
DZP	$GABA_AR$	−7.2	1.842	Tyr-58C	Hydrophobic	3.52
				Phe77C	Hydrophobic	3.47
				Phe100D	Hydrophobic	3.83
				Phe100D	Hydrophobic	3.92
				Tyr160D	Hydrophobic	3.56
				Val203D	Hydrophobic	3.95
				Tyr210D	Hydrophobic	3.38
				Tyr210D	Hydrophobic	3.86
				SER-205D	H-bond	2.94
				SER-206D	H-bond	3.16
				His-102D	Halogen Bond	3.82
CAMEL	CAII	−7.1	1.858	Ile-91	Hydrophobic	3.33
				Gln-92	Hydrophobic	3.85
				Asp-130	Hydrophobic	3.84
				Phe-131	Hydrophobic	3.56
				Phe-131	Hydrophobic	3.37
				Leu-198	Hydrophobic	3.37
				Gln-92	H-bond	2.98
				Thr-199	H-bond	2.97
				Thr-200	H-bond	2.20
				Thr-200	H-bond	2.00
				Phe-131	π-Stacking-P	4.05
				His-94	Salt Bridge	4.42
				His-96	Salt Bridge	5.19
				His-119	Salt Bridge	5.34
TE1	CAII	−5.4	1.91	Ile-91	Hydrophobic	3.66
				Gln-92	Hydrophobic	3.60
				Arg-58	H-bond	3.34
				Asn-67	H-bond	1.44
				Gln-92	H-bond	2.35
				Phe-131	π-Stacking-T	4.76

Table 4
Physicochemical properties calculated by the ADMETlab server and analyzed by the CNS MPO algorithm from Pfizer, Inc.

Property	Value	T0
logP	2.60	1.00
$logD_{7.4}$	2.33	0.83
MW	366.33 g mol^{-1}	0.00
TPSA	126.61 $Å^2$	0.95
HBD	2	0.50
pKa (basic)	0.63	1.00
CNS MPO score	4.3	
Pfizer rule	Accepted	
Golden Triangle rule	Accepted	

Permeability Assay (PAMPA) expressed in Papp MDCK for BBB permeability, and Papp Caco-2 for gastrointestinal permeability were predicted [49]. Where Papp values on the order of 10^{-5} cm/s are compounds with high cell permeability, according to Pfizer, Inc.'s biopharmaceutical classification system [50]. When aligned with logP < 3, the polar surface area of 126.61 $Å^2$ causes CAMEL to reside in a physicochemical space formed by compounds with optimized CNS permeability properties with low risk of neurotoxic response (Fig. 10c) from in vivo assays [51], agreeing with the predicted value of Papp MDCK on the order of 1.4×10^{-5} cm/s, indicating that the compound can be distributed to the CNS by BBB permeability (Table 5). In the Golden Triangle graph (Fig. 10d), it is possible to notice that the compound resides in a central trend of the physicochemical space formed by MW < 400 g mol^{-1} and lipophilicity of the deprotonated species at physiological pH (logD at pH 7.4 between 2 and 3), formed by compounds that are permeable in Caco-2 cells and exhibit metabolic stability. This result corroborates with the predicted value of Papp Caco-2 on the order of 2.0×10^{-6} cm/s, indicating that CAMEL is gradually absorbed in the gastrointestinal tract (Table 5). When estimating a probability of 0.99 (on a scale from 0.0 to 1.0) of the compound presenting high passive efflux (Peff), a PAMPA profile was predicted that can reduce the absorbed fraction by < 90 %, while the predicted VD of 0.21 L/kg is indicative that the anionic species of CAMEL has a greater affinity with blood plasma than in biological tissues (Table 5). Such analysis suggests that CNS activity is observed in a basal effect, expressing a gradual permeability in biological membranes, including the blood-brain barrier [52]. Additionally, ionization can affect the pharmacokinetic speed of CAMEL, although it does not negatively affect the overall DMPK profile.

3.8.3. *Human liver microsome (HLM) stability*

Predicting the drug metabolism sites is a crucial analysis step that accounts for 39 % of failures in clinical trials. This prediction helps us estimate the toxic effects of secondary metabolites formed from hepatic metabolism conducted by the CYP450 isoenzymes. One of these

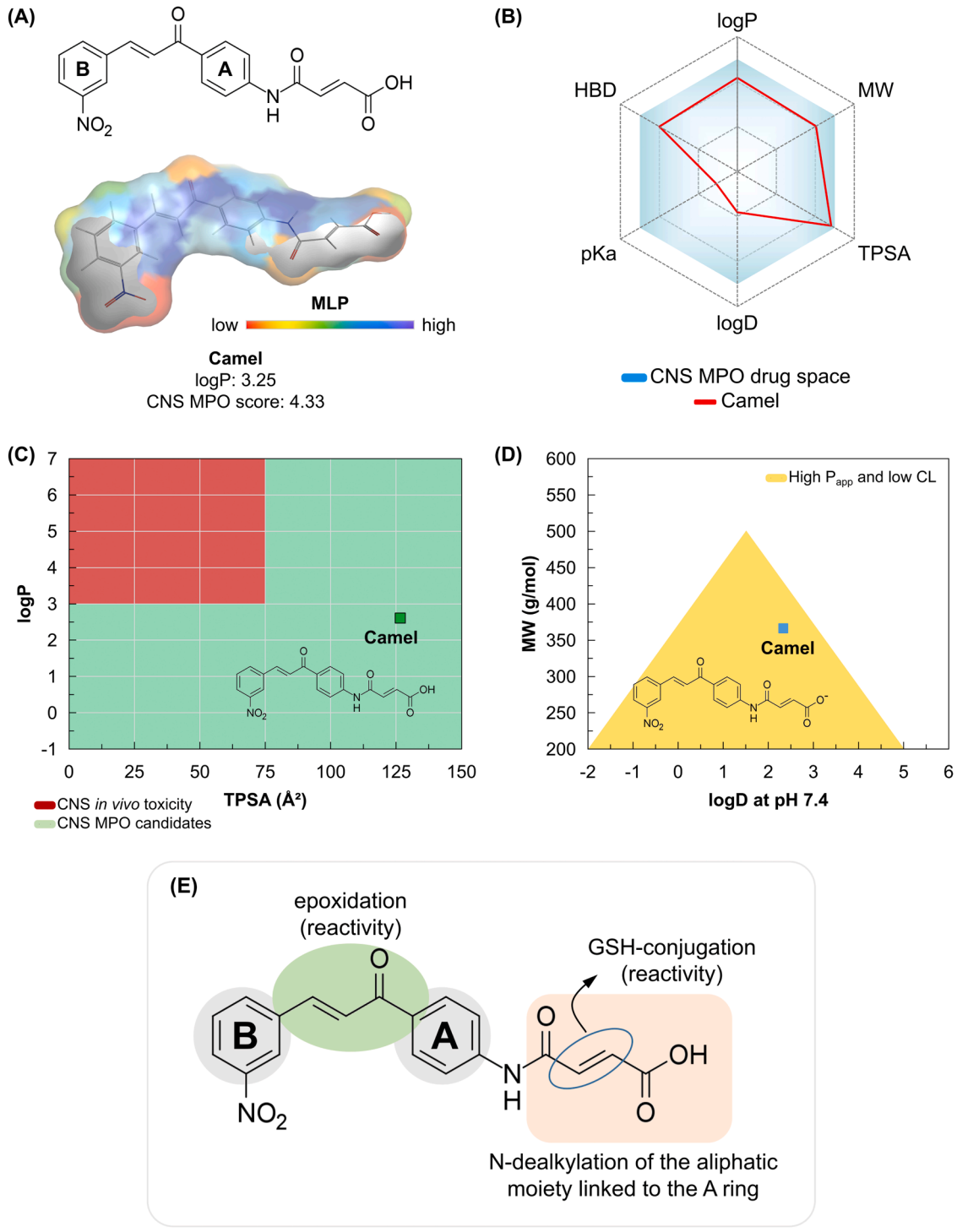

Fig. 10. (A) Lipophilicity and polarity analysis by MLP, (B) druglikeness radar by MPO analysis, (C) alignment between logP and TPSA for analysis of CNS activity, (D) alignment between MW and logD for estimation of cell viability profile and (E) prediction of metabolism site.

metabolites is based on the formation of epoxides, which are unstable intermediates resulting from the hydroxylation of unsaturated centers. Their reactivity can lead to damage caused by the formation of covalent bonds in macromolecules such as DNA and proteins.

In this prediction, it was observed that CAMEL is primarily metabolized by the CYP2C9 isoform in hepatic phase I metabolism, with the biotransformation site located in the aliphatic side chain linked to the para-substituted nitrogen in ring A, through N-dealkylation reactions. The intrinsic fraction released in the plasma can undergo biotransformation through GSH-conjugation reactions in phase II metabolism, with the metabolism site located in the unsaturated system between the amide and carboxyl groups of the aliphatic substructure linked to ring A, reducing the reactivity of this group when binding to undesirable macromolecules. However, the α,β-unsaturated aliphatic system between rings A and B constitutes a hydroxylation site, and the resulting epoxidized intermediate can be reactive, leading to the probability of inducing liver damage. When the stability descriptors of HLM were analyzed, it was observed that the predicted value of CLHepa in the order of 3.9×10^{-2} μL.min-1(106 cells)−1 indicates low clearance due to slow metabolism, consistent with the predicted CLPlasma of 5.37 mL/

Table 5
DMPK properties predicted using PreADMET, ADMETlab and ADMETboost tools, expressed in PAMPA descriptors and HLM stability.

Property	Value	Source
P_{app} MDCK	1.4×10^{-5} cm/s	ADMETlab
P_{app} Caco-2	2.0×10^{-6} cm/s	PreADMET
PAMPA (P_{eff})	0.99	ADMETlab
Fraction absorbed (%)	87.93 %	PreADMET
VD	0.21 L/kg	ADMETlab
CYP2C9 substrate	0.93	ADMETlab
CYP2D6 substrate	0.25	ADMETlab
CYP3A4 substrate	0.05	ADMETlab
CL_{Plasma}	5.37 mL/min/kg	ADMETlab
CL_{Hepa}	3.9×10^{-2} μL.min^{-1}(10^6 cells)$^{-1}$	ADMETboost
HLM (< 30 min)	0.16	ADMETlab
DILI	1.00	ADMETlab

min/kg, which is ideal for ensuring a viable half-life (Fig. 10e). Thus, a low probability of HLM stability resulting in clearance in < 30 min was predicted, based on the stability of CAMEL phase I metabolism (Table 5).

4. Conclusion

DFT calculations were done and finding the lowest energy conformer through rotations around the C9′ - C1′ bond axis, the lowest energy structures show a non-planar conformation. The ^{1}H and ^{13}C NMR analyses helped figure out the molecular structure of the new chalcone made, and then confirmed it using quantum chemical calculations, which matched up well with the actual chemical shifts. The electronic transition HOMO-LUMO happens between π – π* orbitals. The energy gap analysis and hardness values higher than softness values confirm the stability of CAMEL, with CGDRs indicating it's more electrophilic in nature. As per MEP results, the regions with higher electronic density are around oxygen atoms due to their high electronegativity, while hydrogens have lower electronic densities. Comparing the chemical behavior in DMSO and water solution showed a similar profile, while comparing vacuum with polar environments revealed an increase in electrophilic character in ring B and nucleophilic character in ring A. The most nucleophilic sites were C1′ and N2, while the most electrophilic were N1, O1, and O2. Experiments concluded that at all doses, the sample was non-toxic and didn't affect the animals' movement at 20 and 40 mg kg^{-1} doses, but at 4 mg kg^{-1}, the fish showed lethargic behavior. Regarding its anxiolytic and anticonvulsant effect, the derivative showed behavior like Diazepam, a major anti-anxiety medication, along with activity via the GABAA pathway. Molecular docking simulations showed that CAMEL had interactions with similar residues followed by a better specificity for the DZP agonist binding site on GABAA receptors and better specificity for the inhibition site compared to TE1 versus CAII, suggesting it could act similarly to DZP and TE1. DMPK analyses indicated that CAMEL has excellent permeability in MDCK and Caco-2 cell lines, aiding gradual access to the CNS through intestinal and cerebral permeability.

Author contributions

All authors have read and agreed to the published version of the manuscript.

CRediT authorship contribution statement

Francisco N.M. Lucio: Data curation. **Akenaton O.C.V. Gomes:** Formal analysis. **Paulo N. Bandeira:** Methodology. **Maria K.A. Ferreira:** Conceptualization. **Walber H.F. Ribeiro:** Validation. **Ivana C. Romão:** Investigation. **Caio H.A. Roberto:** Visualization. **Marcia M. Marinho:** Software. **Alexandre M.R. Teixeira:** Writing – review & editing. **Emmanuel S. Marinho:** Writing – original draft. **Andreia F.C. de Gomes:** Writing – review & editing. **Jane E.S.A. de Menezes:** Resources. **Hélcio S. dos Santos:** Writing – original draft, Supervision, Resources.

Declaration of competing interest

The authors declare that they have no known competing financial interests or personal relationships that could have appeared to influence the work reported in this paper.

Acknowledgments

We thank the Northeastern Center for the Application and Use of Nuclear Magnetic Resonance (CENAUREMN) for the NMR measurements, and the Department of Physics of the Federal University of Ceará for the ATR-FTIR measurements. Financial support from Fundação Cearense de Apoio ao Desenvolvimento Científico e Tecnológico (FUNCAP), Coordenação de Aperfeiçoamento de Pessoal de Nível Superior (CAPES) and Conselho Nacional de Desenvolvimento Científico e Tecnológico (CNPq) is also acknowledged. Hélcio Silva dos Santos acknowledges financial support from the PQ/CNPq (Grant#: 306008/2022–0), FUNCAP (Grants#: ITR-0214–00060.01.00/23, UNI-0210–00337.01.00/23, FPD-0213–00088.01.00/23), and Alexandre M. R. Teixeira acknowledges financial support from the PQ/CNPq (Grant#: 308178/2021–1), and from the FUNCAP (Grants#: UNI-0210–00315.01.00/23 and FPD-0213–00191.01.00/23).

Supplementary materials

Supplementary material associated with this article can be found, in the online version, at doi:10.1016/j.molstruc.2024.140466.

Data availability

Data will be made available on request.

References

[1] S.M. Testa, J. Brandt, Do patients with psychogenic nonepileptic seizures have positive covert attitudes toward sickness? Epileps. Behav. 19 (2010) 323–327, https://doi.org/10.1016/j.yebeh.2010.07.014.
[2] J.A. Salpekar, T. Basu, S. Thangaraj, J. Maguire, The intersections of stress, anxiety and epilepsy, Int. Rev. Neurobiol., Elsevier (2020) 195–219, https://doi.org/10.1016/bs.irn.2020.02.001.
[3] Y.C. Chen, M. Priyadarshini, P. Panula, Complementary developmental expression of the two tyrosine hydroxylase transcripts in zebrafish, Histochem. Cell Biol. 132 (2009) 375–381, https://doi.org/10.1007/s00418-009-0619-8.
[4] M.K.A. Ferreira, R.O.S. Fontenelle, F.E.A. Magalhães, P.N. Bandeira, J.E. Silva A. De Menezes, H.S. Dos Santos, Chalcones pharmacological potential: a brief review, Rev. Virtual Quim. 10 (2018) 1455–1473, https://doi.org/10.21577/1984-6835.20180099.
[5] P. Padaratz, M. Fracasso, F. De Campos-Buzzi, R. Corrêa, R. Niero, F.D. Monache, V. Cechinel-Filho, Antinociceptive activity of a new benzofuranone derived from a chalcone, Basic Clin. Pharma. Tox. 105 (2009) 257–261, https://doi.org/10.1111/j.1742-7843.2009.00441.x.
[6] R. Corrêa, M.A.S. Pereira, D. Buffon, L. Dos Santos, V.C. Filho, A.R.S. Santos, R. J. Nunes, Antinociceptive properties of chalcones. Structure-activity relationships, Arch. Pharm. Pharm. Med. Chem. 334 (2001) 332–334, https://doi.org/10.1002/1521-4184(200110)334:10<332::AID-ARDP332>3.0.CO;2-O.
[7] F. De Campos-Buzzi, J. Pereira De Campos, P. Pozza Tonini, R. Corrêa, R. Augusto Yunes, P. Boeck, V. Cechinel-Filho, Antinociceptive effects of synthetic chalcones obtained from Xanthoxyline, Arch. Pharm. (Weinheim) 339 (2006) 361–365, https://doi.org/10.1002/ardp.200600049.
[8] Z. Nowakowska, A review of anti-infective and anti-inflammatory chalcones, Eur. J. Med. Chem. 42 (2007) 125–137, https://doi.org/10.1016/j.ejmech.2006.09.019.
[9] F. De Campos-Buzzi, P. Padaratz, A. Meira, R. Corrêa, R. Nunes, V. Cechinel-Filho, 4'-acetamidochalcone derivatives as potential antinociceptive agents, Molecules. 12 (2007) 896–906, https://doi.org/10.3390/12040896.
[10] C. Karthikeyan, N.S.H. Narayana Moorthy, S. Ramasamy, U. Vanam, E. Manivannan, D. Karunagaran, P. Trivedi, Advances in chalcones with anticancer activities, PRA 10 (2014) 97–115, https://doi.org/10.2174/1574892809666140819153902.
[11] P. Teixeira Da Silva, L. Mesquita Albuquerque Lopes, J. Da Cunha Xavier, M. Costa S. De Carvalho, M. Odorico De Moraes, C. Pessoa, F. Washington Araujo Barros-Nepomuceno, P. Nogueira Bandeira, C. Sidrim De Paula Cavalcante Targino,

A. Magno Rodrigues Teixeira, R. Oliveira Dos Santos Fontenelle, H. Silva Santos, Cytotoxic and antifungal activity of chalcones synthesized from natural acetophenone isolated from croton anisodontus, Rev. Virtual Quim. 12 (2020) 712–723, https://doi.org/10.21577/1984-6835.20200057.
[12] A.M.R. Teixeira, H.S. Santos, P.N. Bandeira, M.S.S. Julião, P.T.C. Freire, V.N. Lima, B.G. Cruz, P.T. Da Silva, H.D.M. Coutinho, D.M. Sena, Structural, spectroscopic and microbiological characterization of the chalcone 2E-1-(2'-hydroxy-3',4',6'-trimethoxyphenyl)-3-(phenyl)-prop-2-en-1-one derived from the natural product 2-hydroxy-3,4,6-trimethoxyacetophenone, J. Mol. Struct. 1179 (2019) 739–748, https://doi.org/10.1016/j.molstruc.2018.11.075.
[13] M.K.A. Ferreira, A.W. Da Silva, F.C.O. Silva, C.L.A. Holanda, S.M. Barroso, J.D. R. Lima, A.E. Vieira Neto, A.R. Campos, P.N. Bandeira, H.S. Dos Santos, T.L.G. De Lemos, S.M.C. Siqueira, F.E.A. Magalhães, J.E.S.A. De Menezes, Anxiolytic-like effect of chalcone N-{(4′-[(E)-3-(4-fluorophenyl)-1-(phenyl) prop-2-en-1-one]} acetamide on adult zebrafish (Danio rerio): involvement of the GABAergic system, Behav. Brain Res. 374 (2019) 111871, https://doi.org/10.1016/j.bbr.2019.03.040.
[14] H.P. Ávila, E.D.F.A. Smânia, F.D. Monache, A. Smânia, Structure–activity relationship of antibacterial chalcones, Bioorg. Med. Chem. 16 (2008) 9790–9794, https://doi.org/10.1016/j.bmc.2008.09.064.
[15] D. Batovska, St. Parushev, A. Slavova, V. Bankova, I. Tsvetkova, M. Ninova, H. Najdenski, Study on the substituents' effects of a series of synthetic chalcones against the yeast Candida albicans, Eur. J. Med. Chem. 42 (2007) 87–92, https://doi.org/10.1016/j.ejmech.2006.08.012.
[16] P. Boeck, C.A. Bandeira Falcão, P.C. Leal, R.A. Yunes, V.C. Filho, E.C. Torres-Santos, B. Rossi-Bergmann, Synthesis of chalcone analogues with increased antileishmanial activity, Bioorg. Med. Chem. 14 (2006) 1538–1545, https://doi.org/10.1016/j.bmc.2005.10.005.
[17] S. Mathew, T.E. Abraham, In vitro antioxidant activity and scavenging effects of Cinnamomum verum leaf extract assayed by different methodologies, Food Chem. Toxicol. 44 (2006) 198–206, https://doi.org/10.1016/j.fct.2005.06.013.
[18] T.R. Garcia, T.S. De Freitas, H.S. Dos Santos, P.N. Bandeira, M.S.S. Julião, J. E. Rocha, C.E.S. Nogueira, R.L.S. Pereira, A.C.H. Barreto, P.T.C. Freire, H.D. M. Coutinho, A.M.R. Teixeira, Structural, vibrational and electrochemical analysis and antibiotic activity study of chalcone (2E)-1-(3',-methoxy-4',-hydroxyphenyl)-3-(3-nitrophenyl)prop-2-en-1-one, J. Mol. Struct. 1216 (2020) 128358, https://doi.org/10.1016/j.molstruc.2020.128358.
[19] K. Nepali, H.-Y. Lee, J.-P. Liou, Nitro-group-containing drugs, J. Med. Chem. 62 (2019) 2851–2893, https://doi.org/10.1021/acs.jmedchem.8b00147.
[20] E.M. Sayed, R. Hassanien, N. Farhan, H.F. Aly, K. Mahmoud, S.K. Mohamed, J. T. Mague, E.A. Bakhite, Nitrophenyl-Group-Containing Heterocycles. I. Synthesis, Characterization, Crystal Structure, Anticancer Activity, and Antioxidant Properties of Some New 5,6,7,8-Tetrahydroisoquinolines Bearing 3(4)-Nitrophenyl Group, ACS. Omega 7 (2022) 8767–8776, https://doi.org/10.1021/acsomega.1c06994.
[21] V.A. Mamedov, V.R. Galimullina, Z.-W. Qu, H. Zhu, V.V. Syakaev, L. R. Shamsutdinova, M.A. Sergeev, I.Kh. Rizvanov, A.T. Gubaidullin, O.G. Sinyashin, S. Grimme, $AlCl_3$ -Promoted Intramolecular Indolinone-Quinolone Rearrangement of Spiro[indoline-3,2′-quinoxaline]-2,3′-diones: easy Access to Quinolino[3,4- *b*] quinoxalin-6-ones, J. Org. Chem. 89 (2024) 898–917, https://doi.org/10.1021/acs.joc.3c01906.
[22] U. Bothe, J. Günther, R. Nubbemeyer, H. Siebeneicher, S. Ring, U. Bömer, M. Peters, A. Rausch, K. Denner, H. Himmel, A. Sutter, I. Terebesi, M. Lange, A. M. Wengner, N. Guimond, T. Thaler, J. Platzek, U. Eberspächer, M. Schäfer, H. Steuber, T.M. Zollner, A. Steinmeyer, N. Schmidt, Discovery of IRAK4 Inhibitors BAY1834845 (Zabedosertib) and BAY1830839, J. Med. Chem. 67 (2024) 1225–1242, https://doi.org/10.1021/acs.jmedchem.3c01714.
[23] S. Wittlin, P. Mäser, From magic bullet to magic bomb: reductive bioactivation of antiparasitic agents, ACS Infect. Dis. 7 (2021) 2777–2786, https://doi.org/10.1021/acsinfecdis.1c00118.
[24] R. Paoli-Lombardo, N. Primas, S. Bourgeade-Delmas, A. Sournia-Saquet, C. Castera-Ducros, I. Jacquet, P. Verhaeghe, P. Rathelot, P. Vanelle, Synthesis of New 5- or 7-Substituted 3-Nitroimidazo[1,2-a]pyridine Derivatives Using SNAr and Palladium-Catalyzed Reactions To Explore Antiparasitic Structure–Activity Relationships, Synthesis (Mass) (2023), https://doi.org/10.1055/a-2232-8113 a-2232-8113.
[25] S.I. Mulla, R.N. Bharagava, D. Belhaj, G.D. Saratale, Z.K. Bagewadi, G. Saxena, A. Kumar, H. Mohan, C.-P. Yu, H.Z. Ninnekar, An overview of nitro group-containing compounds and herbicides degradation in microorganisms, in: P. K. Arora (Ed.), Microbial Metabolism of Xenobiotic Compounds, Springer Singapore, Singapore, 2019, pp. 319–335, https://doi.org/10.1007/978-981-13-7462-3_16.
[26] M.K.A. Ferreira, A.W. Da Silva, F.C.O. Silva, A.E. Vieira Neto, A.R. Campos, S. A. Alves Rodrigues Santos, A.M. Rodrigues Teixeira, J. Da Cunha Xavier, P. N. Bandeira, C.E. Sampaio Nogueira, D.H.A. De Brito, E.L. Rebouças, F.E. A. Magalhães, J.E.S.A. De Menezes, H.S. Dos Santos, Anxiolytic-like effect of chalcone N-{4'[(2E)-3-(3-nitrophenyl)-1-(phenyl)prop-2-en-1-one]} acetamide on adult zebrafish (Danio rerio): involvement of the 5-HT system, Biochem. Biophys. Res. Commun. 526 (2020) 505–511, https://doi.org/10.1016/j.bbrc.2020.03.129.
[27] T. Rodrigues Garcia, P.D.T.C. Freire, A.W. Da Silva, M.K.A. Ferreira, E.D. L. Rebouças, F.R.S. Mendes, E.M. Marinho, M.M. Marinho, A.M.R. Teixeira, E. S. Marinho, P.N. Bandeira, J.E.S.A. De Menezes, H.S. Dos Santos, Anxiolytic and anticonvulsant effect of Ibuprofen derivative through GABAergic neuromodulation in adult Zebrafish, J. Biomol. Struct. Dyn. 41 (2023) 12055–12062, https://doi.org/10.1080/07391102.2023.2170915.
[28] A.D. Becke, Density-functional thermochemistry. I. The effect of the exchange-only gradient correction, J. Chem. Phys. 96 (1992) 2155–2160, https://doi.org/10.1063/1.462066.
[29] C. Lee, W. Yang, R.G. Parr, Development of the Colle-Salvetti correlation-energy formula into a functional of the electron density, Phys. Rev. B 37 (1988) 785–789, https://doi.org/10.1103/PhysRevB.37.785.
[30] M.J. Frisch, gaussian09, http://www.Gaussian.Com/ (2009).
[31] E. Cancès, B. Mennucci, J. Tomasi, A new integral equation formalism for the polarizable continuum model: theoretical background and applications to isotropic and anisotropic dielectrics, J. Chem. Phys. 107 (1997) 3032–3041, https://doi.org/10.1063/1.474659.
[32] R.P. Iczkowski, J.L. Margrave, Electronegativity, J. Am. Chem. Soc. 83 (1961) 3547–3551, https://doi.org/10.1021/ja01478a001.
[33] R.G. Pearson, Recent advances in the concept of hard and soft acids and bases, J. Chem. Educ. 64 (1987) 561, https://doi.org/10.1021/ed064p561.
[34] R.G. Parr, L.V. Szentpály, S. Liu, Electrophilicity Index, J. Am. Chem. Soc. 121 (1999) 1922–1924, https://doi.org/10.1021/ja983494x.
[35] R.G. Pearson, Hard and Soft Acids and Bases, J. Am. Chem. Soc. 85 (1963) 3533–3539, https://doi.org/10.1021/ja00905a001.
[36] P.K. Chattaraj, S. Giri, S. Duley, Update 2 of: electrophilicity Index, Chem. Rev. 111 (2011) PR43–PR75, https://doi.org/10.1021/cr100149p.
[37] F.W.Q. Almeida-Neto, L.P. da Silva, M.K.A. Ferreira, F.R.S. Mendes, K.K.A. de Castro, P.N. Bandeira, J.E.S.A. de Menezes, H.S. dos Santos, N.K.V. Monteiro, E. S. Marinho, P. de Lima-Neto, Characterization of the structural, spectroscopic, nonlinear optical, electronic properties and antioxidant activity of the N-{4'-[(E)-3-(Fluorophenyl)-1-(phenyl)-prop-2-en-1-one]}-acetamide, J. Mol. Struct. 1220 (2020) 128765, https://doi.org/10.1016/j.molstruc.2020.128765.
[38] A.W. Da Silva, M.K.A. Ferreira, L.R. Pereira, E.L. Rebouças, M.R. Coutinho, J. Dos, R. Lima, M.I.F. Guedes, P.N. Bandeira, F.E.A. Magalhães, J.E.S.A.D. Menezes, M. M. Marinho, A.M.R. Teixeira, M.T. Salles Trevisan, H.S. Dos Santos, E.S. Marinho, *Combretum lanceolatum* extract reverses anxiety and seizure behavior in adult zebrafish through GABAergic neurotransmission: an in vivo *and in silico* study, J. Biomol. Struct. Dyn. 40 (2022) 9801–9814, https://doi.org/10.1080/07391102.2021.1935322.
[39] A. Maresca, C. Temperini, H. Vu, N.B. Pham, S.-A. Poulsen, A. Scozzafava, R. J. Quinn, C.T. Supuran, Non-zinc mediated inhibition of carbonic anhydrases: coumarins are a new class of suicide inhibitors, J. Am. Chem. Soc. 131 (2009) 3057–3062, https://doi.org/10.1021/ja809683v.
[40] S. Masiulis, R. Desai, T. Uchański, I. Serna Martin, D. Laverty, D. Karia, T. Malinauskas, J. Zivanov, E. Pardon, A. Kotecha, J. Steyaert, K.W. Miller, A. R. Aricescu, GABAA receptor signalling mechanisms revealed by structural pharmacology, Nature 565 (2019) 454–459, https://doi.org/10.1038/s41586-018-0832-5.
[41] O. Trott, A.J. Olson, AutoDock Vina: improving the speed and accuracy of docking with a new scoring function, efficient optimization, and multithreading, J. Comput. Chem. 31 (2010) 455–461, https://doi.org/10.1002/jcc.21334.
[42] V.M. De Oliveira, M.N. Da Rocha, C.H.A. Roberto, F.N.M. Lucio, M.M. Marinho, E. S. Marinho, S.M. De Morais, Insights of structure-based virtual screening and MPO-based SAR analysis of berberine-benzimidazole derivatives against Parkinson disease, J. Mol. Struct. 1302 (2024) 137453, https://doi.org/10.1016/j.molstruc.2023.137453.
[43] I.K. Campos Lima, F.N.M. Lucio, A.O.C.V. Gomes, H.D.M. Coutinho, F.F. Mesquita Cajazeiras, J.E. Rocha, J.M. Guedes, M. Nunes Da Rocha, M.M. Marinho, K.M. Canuto, L.M. Alexandre E Silva, A.M. Rodrigues Teixeira, E.S. Marinho, H.S. Dos Santos, M.S.D.S. Julião, Structural characterization, Dft calculations, Admet studies, antibiotic potentiating activity, evaluation of efflux pump inhibition of hydrazone derivative of the drug hydralazine, (2024). https://doi.org/10.2139/ssrn.4775685.
[44] A.W. Da Silva, M.K.A Ferreira, E.L. Reboucas, F.C.O Silva, C.L.A Holanda, S. M. Barroso, J.D. Reis Lima, F.L.A Batista, F.R.S Mendes, A.R. Campos, J.E.S. De Menezes, F.E.A Magalhaes, S.M.C Siqueira, H.S. Dos Santos, Anxiolytic-like effect of Azadirachta indica A. Juss. (Neem, Meliaceae) bark on adult zebrafish (Danio rerio): participation of the Serotoninergic and GABAergic systems, PPIJ 8 (2020) 256–263, https://doi.org/10.15406/ppij.2020.08.00303.
[45] D.L. Gebauer, N. Pagnussat, Â.L. Piato, I.C. Schaefer, C.D. Bonan, D.R. Lara, Effects of anxiolytics in zebrafish: similarities and differences between benzodiazepines, buspirone and ethanol, Pharmacol. Biochem. Behav. 99 (2011) 480–486, https://doi.org/10.1016/j.pbb.2011.04.021.
[46] F. Ahmad, M.K. Richardson, Exploratory behaviour in the open field test adapted for larval zebrafish: impact of environmental complexity, Behav. Processes 92 (2013) 88–98, https://doi.org/10.1016/j.beproc.2012.10.014.
[47] P. Tirassa, N. Costa, L. Aloe, CCK-8 prevents the development of kindling and regulates the GABA and NPY expression in the hippocampus of pentylenetetrazole (PTZ)-treated adult rats, Neuropharmacology. 48 (2005) 732–742, https://doi.org/10.1016/j.neuropharm.2004.12.001.
[48] T.T. Wager, R.Y. Chandrasekaran, X. Hou, M.D. Troutman, P.R. Verhoest, A. Villalobos, Y. Will, Defining Desirable central nervous system drug space through the alignment of molecular properties, in Vitro ADME, and safety attributes, ACS Chem. Neurosci. 1 (2010) 420–434, https://doi.org/10.1021/cn100007x.
[49] A. Fortuna, G. Alves, P. Soares-Da-Silva, A. Falcão, Optimization of a parallel artificial membrane permeability assay for the fast and simultaneous prediction of human intestinal absorption and plasma protein binding of drug candidates: application to Dibenz[b,f]azepine-5-Carboxamide derivatives, J. Pharm. Sci 101 (2012) 530–540, https://doi.org/10.1002/jps.22796.
[50] M. Pettersson, X. Hou, M. Kuhn, T.T. Wager, G.W. Kauffman, P.R. Verhoest, Quantitative assessment of the impact of fluorine substitution on P-glycoprotein (P-

gp) mediated efflux, permeability, lipophilicity, and metabolic stability, J. Med. Chem. 59 (2016) 5284–5296, https://doi.org/10.1021/acs.jmedchem.6b00027.
[51] J.D. Hughes, J. Blagg, D.A. Price, S. Bailey, G.A. DeCrescenzo, R.V. Devraj, E. Ellsworth, Y.M. Fobian, M.E. Gibbs, R.W. Gilles, N. Greene, E. Huang, T. Krieger-Burke, J. Loesel, T. Wager, L. Whiteley, Y. Zhang, Physiochemical drug properties associated with in vivo toxicological outcomes, Bioorg. Med. Chem. Lett. 18 (2008) 4872–4875, https://doi.org/10.1016/j.bmcl.2008.07.071.
[52] D.E.V. Pires, L.M. Kaminskas, D.B. Ascher, Prediction and optimization of pharmacokinetic and toxicity properties of the ligand, in: M. Gore, U.B. Jagtap (Eds.), Computational Drug Discovery and Design, Springer New York, New York, NY, 2018, pp. 271–284, https://doi.org/10.1007/978-1-4939-7756-7_14.